REPORT DOCUMENTATION PAGE

Form Approved
OMB No. 0704-0188

(2)

AD-A231 692

2. REPORT DATE	3. REPORT TYPE AND DATES COVERED
DEC 1990	FINAL

4. TITLE AND SUBTITLE
THE EFFECT OF REMOTE SENSOR SPATIAL RESOLUTION IN MONITORING U.S ARMY TRAINING MANEUVER SITES.

5. FUNDING NUMBERS

6. AUTHOR(S)
HARRY L. CUNNINGHAM

7. PERFORMING ORGANIZATION NAME(S) AND ADDRESS(ES)
HARRY L. CUNNINGHAM
DEPARTMENT OF FOREST AND WOOD SCIENCES
COLORADO STATE UNIVERSITY
FORT COLLINS, CO 80523

8. PERFORMING ORGANIZATION REPORT NUMBER

9. SPONSORING/MONITORING AGENCY NAME(S) AND ADDRESS(ES)
U.S. ARMY STUDENT DETACHMENT
FORT BENJAMIN HARRISON, INDIANA

10. SPONSORING/MONITORING AGENCY REPORT NUMBER

11. SUPPLEMENTARY NOTES

12a. DISTRIBUTION/AVAILABILITY STATEMENT
APPROVED FOR PUBLIC RELEASE; DISTRIBUTION UNLIMITED

12b. DISTRIBUTION CODE

13. ABSTRACT (Maximum 200 words)
NINE SETS OF REMOTE SENSOR DATA CONSISTING OF DIGITIZED AERIAL PHOTOGRAPHY, AIRCRAFT MSS, SPOT AND LANDSAT TM WERE OBTAINED OVER A PORTION OF A U.S. ARMY TRAINING MANEUVER SITE (PINON CANYON) IN SOUTHEASTERN COLORADO. THESE WERE PROCESSED USING 19 DIFFERENT LINE AND EDGE ENHANCEMENT TECHNIQUES TO AID IN THE DETECTION OF OFF-ROAD VEHICULAR DAMAGE (TANK TRAILS). IN ADDITION, A CLASSIFICATION ACCURACY ASSESSMENT WAS CONDUCTED BETWEEN LANDSAT TM AND THE AIRBORNE MSS WITH 6.5 METER SPATIAL RESOLUTION. A WEIGHTED LAPLACIAN FILTER WAS THE MOST EFFECTIVE AND TIME EFFICIENT ENHANCEMENT TECHNIQUE. GEOSCAN'S MK II AIRBORNE MSS WAS THE MOST EFFECTIVE DIGITAL DATA SET FOR ENHANCING TANK TRAILS. HOWEVER, IT ONLY RESOLVED 65-70% OF THE TANK TRAILS PRESENT IN HIGH-QUALITY AERIAL PHOTOGRAPHY. THEREFORE, HIGH-QUALITY AERIAL PHOTOGRAPHY WILL PROVIDE THE MOST INFORMATION REGARDING OFF-ROAD VEHICULAR DAMAGE. LANDSAT TM CLASSIFIED FOREST COVER TYPES WITH A HIGHER DEGREE OF ACCURACY AS COMPARED TO THE HIGHER RESOLUTION AIRBORNE MSS. THIS IS DUE TO THE HIGH SPECTRAL VARIABILITY PRESENT IN A FOREST CANOPY. THERE WAS NO SIGNIFICANT DIFFERENCE IN CLASSIFICATION ACCURACY FOR GRASS COVER TYPES DUE TO THE LACK OF SPECTRAL VARIANCE FROM PIXEL TO PIXEL.

14. SUBJECT TERMS
SPATIAL RESOLUTION, IMAGE ENHANCEMENT TECHNIQUES, OFF-ROAD VEHICULAR DAMAGE, CLASSIFICATION ACCURACY ASSESSMENT, AIRBORNE MSS

15. NUMBER OF PAGES
148

16. PRICE CODE

17. SECURITY CLASSIFICATION OF REPORT	18. SECURITY CLASSIFICATION OF THIS PAGE	19. SECURITY CLASSIFICATION OF ABSTRACT	20. LIMITATION OF ABSTRACT
UNCLASSIFIED	UNCLASSIFIED	UNCLASSIFIED	SAR

THESIS

THE EFFECT OF REMOTE SENSOR SPATIAL RESOLUTION IN MONITORING U.S. ARMY TRAINING MANEUVER SITES

Submitted by

Harry L. Cunningham

Department of Forest and Wood Sciences

In partial fulfillment of the requirements

for the degree of Master of Science

Colorado State University

Fort Collins, Colorado

Fall 1990

COLORADO STATE UNIVERSITY

October 31, 1990

WE HEREBY RECOMMEND THAT THE THESIS PREPARED UNDER OUR SUPERVISION BY HARRY L. CUNNINGHAM ENTITLED THE EFFECT OF REMOTE SENSOR SPATIAL RESOLUTION IN MONITORING U.S. ARMY TRAINING MANEUVER SITES BE ACCEPTED AS FULFILLING IN PART REQUIREMENTS FOR THE DEGREE OF MASTER OF SCIENCE.

Committee on Graduate Work

Adviser

Department Head

ABSTRACT OF THESIS

THE EFFECT OF REMOTE SENSOR SPATIAL RESOLUTION
IN MONITORING U.S. ARMY TRAINING MANEUVER SITES

Several types of remote sensor data having different spatial resolutions were obtained over a portion of Pinon Canyon Maneuver Site in Southeastern Colorado to: 1) evaluate the ability of several line and edge enhancement techniques to enhance remote sensor data with different spatial resolutions for the detection of off-road vehicular damage (tank trails), and 2) to observe changes in classification accuracy of a rangeland environment as a function of the sensor spatial resolution and cover type involved.

A weighted Laplacian filter was the most effective and time efficient enhancement technique used for enhancing remote sensor digital data. Geoscan's MKII Airborne Multispectral Scanner with 6.5 meter spatial resolution provided the most effective digital data set for enhancing tank trails. However, this Airborne Scanner data resolved only 65-70% of the tank trails visible in aerial photography obtained by the National Aerial Photography Program (NAPP). Most of this loss of detail occurred in very small trails that were trafficked perhaps only once. Therefore, traditional photointerpretation techniques of high quality aerial photography will provide the

most information regarding off-road vehicular damage, especially minimal damage of small areal extent.

Results of the classification procedure for Airborne Scanner data and Landsat TM data produced overall classification accuracies of 75% and 78%, respectively, for specific classes within major cover type groups (i.e., forest, grass, roads/exposed soil). When major cover type groups were combined, classification accuracy increased to 85% and 91% for the Airborne Scanner and Landsat TM, respectively. In every case, Landsat TM produced higher overall classification results. However, these differences were not significant (α = .01) when all major cover type groups were combined.

When only forest cover types were considered, Landsat TM produced significantly higher results than the Airborne Scanner (α = .01). This result was due to the ability of the lower spatial resolution Landsat TM to average the natural variability in forest canopies within individual pixels. The higher spatial resolution of the Airborne Scanner resulted in higher pixel to pixel variability, thus reducing classification accuracy for cover types of high spectral variability (i.e., forest cover types).

When only roads/exposed soil were considered, the Airborne Scanner produced significantly higher results than Landsat TM (α = .01). This result was due to a higher proportion of the smaller pixels being included completely within the boundary of the cover type, with a smaller proportion of pixels being boundary pixels.

There was no significant difference (α = .01) in classification accuracies between the two sensors when only grass cover types were considered. This result is because the variability from pixel to pixel is approximately the same for grass cover types, irrespective of pixel size. Thus, the 6.5 meter spatial resolution Airborne Scanner achieved similar results as the 25 meter spatial resolution Landsat Thematic Mapper for grass cover types.

This research provides significant results for the U.S. Army and other agencies interested in monitoring semi-arid rangeland environments using remote sensor data.

Harry L. Cunningham
Department of Forest and
Wood Sciences
Colorado State University
Fort Collins, CO 80523
Fall 1990

ACKNOWLEDGEMENTS

Funding and technical support for this research were provided by the U.S. Army Corps of Engineers Cold Regions Research Engineering Laboratory (USACRREL), Hanover, New Hampshire. Specifically, the Research Division, Geological Sciences Branch provided travel expenses, all remote sensor digital data, and the NAPP and NHAP aerial photography used in this research. I am deeply grateful to all the personnel at CRREL who assisted in any way to the success of this research.

Additional support from the Natural Resources Branch of the Directorate of Engineering and Housing, Fort Carson, Colorado, is gratefully acknowledged. Specifically, funding and support of the Land Condition Trend Analysis (LCTA) program at Pinon Canyon Maneuver Site is appreciated. The very detailed information from several LCTA plots was invaluable to the completion of this research. The work of many individuals comprising field crews for the LCTA program is acknowledged and appreciated.

Support from personnel in the Department of Range Science at Colorado State University, including field crews who spent many long, hot days at Pinon Canyon is appreciated.

To my Major Professor, Dr. Roger Hoffer, I am deeply grateful. Without his sage wisdom and advise, this research

would not have been a success. I am also indebted to my other Committee Members, Dr. Joseph Berry and Dr. Freeman Smith for their council and advice. Their suggestions contributed greatly to the quality of this research.

I am also grateful to the Department of Earth Sciences, Dartmouth College, Hanover, New Hampshire for the use of their remote sensing laboratory and equipment during the first stages of this research. Dr. Richard W. Birnie was always available and ready to help when suggestions and guidance were needed. I am grateful to him for cheerfully sharing his time and talents. I would also like to thank Ms. Emily Bryant for the many hours she spent attempting to download the remote sensor data contained on computer compatible tapes that were used in this research. She readily shared her knowledge of remote sensing technology and provided a wealth of invaluable information that will be useful for years to come.

I would like to specifically thank three individuals for the help they have rendered to me during the course of this research. Major (Promotable) William Doe provided the encouragement and direction that was necessary to start and finish this research. I am grateful to him for being a true mentor and friend. Mr. Su He of the Grassland Research Institute, Hohhot, Inner Mongolia, People's Republic of China, and Mr. Vicente Paulo Soares, a graduate student at Colorado State University, deserve a special thanks. Together, they spent many long, arduous hours applying different enhancement

techniques to the remote sensor data used in this research. Their evaluations, suggestions and assistance are acknowledged and deeply appreciated.

Dr. Raymond L. Czaplewski, a mathematical statistician for the USDA Forest Service provided suggestions regarding statistical evaluations for which I am thankful. Additionally, for sharing their insight and knowledge about remote sensing and image processing, I am indebted to Dr. Kyusung Lee and Dr. Yousif Hussin.

I would also like to thank all those who assisted as interpreters in evaluating the different enhancement techniques used in this research. Their contributions to this research were very significant.

Finally, words fail to adequately express my appreciation and love to my wife and children for their support during the course of this research. Their love and encouragement were deeply appreciated when they were so often needed.

TABLE OF CONTENTS

	PAGE
List of Tables	xi
List of Figures	xiii
Chapter 1 - INTRODUCTION	1
1.1 Overview	1
1.2 Objectives	5
Chapter 2 - LITERATURE REVIEW	7
2.1 Effects of Off-Road Vehicular Travel	7
2.2 Remote Sensing and Off-Road Vehicular Travel	8
2.3 Edge and Line Enhancement Techniques	9
2.3.1 Linear Edge Detection Techniques	10
2.3.2 Nonlinear Edge Detection Techniques	14
2.4 Spatial Resolution Considerations	16
2.5 Spatial Resolution and Classification Accuracy	18
2.6 Data Compression Through Principal Components Analysis	21
2.7 Selective Principal Components Analysis	22
Chapter 3 - METHODS AND MATERIALS	24
3.1 Study Areas	24
3.2 Data Used	26
3.3 Detection of Off-Road Vehicular Damage	30
3.3.1 Data Used for Detection of Tank Trails	31
3.3.2 Image Enhancement Techniques	33
3.3.3 Method of Evaluation	39
3.4 Classification Comparison of Two Sensors	41
3.4.1 Use of Normalized Difference Vegetation Index	41
3.4.2 Classification Procedure	43
3.4.3 Evaluation of Classification Accuracy	44
3.4.4 Interrelationships of Sensor Spatial Resolution	46

Chapter 4 - RESULTS AND DISCUSSION. 48

4.1 Detection of Off-Road Vehicular Damage 48

4.1.1 Aerial Photography and Multispectral Scanner Comparison. 62
4.1.2 Relative Cost Comparisons 65

4.2 Classification Comparison of Two Sensors 67

4.2.1 Classification Comparison 72
4.2.2 Tests for Differences in Classification Accuracy. 79

4.3 Interrelationships of Sensor Spatial Resolution. . 84

Chapter 5 - SUMMARY AND CONCLUSIONS 93

5.1 Significant Results. 93
5.2 Applicability of Results 101
5.3 Recommended Topics for Future Research 102

REFERENCES CITED. 106

APPENDICES. 115

Appendix 1 116
Appendix 2 118
Appendix 3 119
Appendix 4 128

LIST OF TABLES

Table		Page
3.1	Pertinent information concerning remote sensor data used in this research	27
3.2	Geoscan's MKII Airborne Multispectral Scanner (AMSS) band specifications.	29
3.3	Matrix used in evaluating enhancement techniques for different remote sensor systems	35
4.1	Matrix used in evaluating enhancement techniques for different remote sensor systems. Asterisks within the cells denote the best enhancement technique for each particular data set	49
4.2	Matrix used in determining the best image and enhancement technique for detection of tank trails. Numbers in matrix refer to image rank as assigned by each individual . .	56
4.3	Performance ranking of images based on responses from interpreters.	59
4.4	Observed interpreter responses classified by image and ranking.	60
4.5	Expected frequencies of interpreter responses if image and ranking were unrelated	60
4.6	Spectral and informational classes for the Airborne Scanner, Study Area 1.	70
4.7	Spectral and informational classes for the Airborne Scanner, Study Area 2.	71
4.8	Spectral and informational classes for the Airborne Scanner, Study Area 3.	71
4.9	Spectral and informational classes for Landsat TM, Study Areas 1-3	72

4.10	Contingency table for classification of the Airborne Scanner data (all three study areas combined)	73
4.11	Contingency table for classification of the Landsat Thematic Mapper data.	74
4.12	Contingency table for combined general cover types for classification of the Airborne Scanner (all study areas combined).	76
4.13	Contingency table for combined general cover types for classification of Landsat TM. . . .	76
4.14	Differences in percent of correctly classified pixels for test areas in the Airborne Scanner and Landsat TM	79
4.15	Mean and standard deviation of forest and grassland cover types for the Airborne Scanner and Landsat TM. Top number is the mean with standard deviation in parentheses	85
A1.1	Land Condition Trend Analysis (LCTA) plot information	116
A2.1	A partial list of dominant vegetation found at Pinon Canyon	118
A4.1	Data used for Kolmogorov-Smirnov goodness-of-fit test for normality for the differences in classification accuracy between the Airborne Scanner and Landsat TM for all major cover type groups combined.	130
A4.2	Data used for Kolmogorov-Smirnov goodness-of-fit test for normality for the differences in classification accuracy between the Airborne Scanner and Landsat TM for forested areas . .	131
A4.3	Data used for Kolmogorov-Smirnov goodness-of-fit test for normality for the differences in classification accuracy between the Airborne Scanner and Landsat TM for roads/exposed soil.	132
A4.4	Data used for Kolmogorov-Smirnov goodness-of-fit test for normality for the differences in classification accuracy between the Airborne Scanner and Landsat TM for grassland areas. .	133

LIST OF FIGURES

Figure		Page
3.1	Location of Pinon Canyon Maneuver Site and selected study areas. (After Shaw et al., 1989).	25
3.2	Spectral band comparison between SPOT Panchromatic, Landsat Thematic Mapper, and Geoscan's MKII Airborne Multispectral Scanner.	28
4.1	Image selected as the best enhanced image from the enlarged NAPP photography (digitized). The Laplacian (Filter 2) filter was used for this enhancement	50
4.2	Image selected as the best enhanced image from the digitized NAPP photography, one band. The Laplacian (Filter 3) filter was used for this enhancement.	50
4.3	Image selected as the best enhanced image from the digitized NAPP photography, three bands. The Laplacian (Filter 2) filter was used for this enhancement.	51
4.4	Image selected as the best enhanced image from the Airborne Multispectral Scanner, one band. The Laplacian (Filter 2) filter was used for this enhancement.	51
4.5	Image selected as the best enhanced image from the Airborne Multispectral Scanner, three bands. The Laplacian (Filter 2) filter was used for this enhancement	52
4.6	Image selected as the best enhanced image from the SPOT Panchromatic data. The high-pass (3 x 3) filter was used for this enhancement.	52
4.7	Image selected as the best enhanced image from the SPOT/TM intensity, hue, saturation transformation data. The high-pass (3 x 3) filter was used for this enhancement	53

4.8 Image selected as the best enhanced image from Landsat Thematic Mapper, one band. The high-pass (3 x 3) filter was used for this enhancement. 53

4.9 Image selected as the best enhanced image from Landsat Thematic Mapper, three bands. The Laplacian (Filter 2) filter was used for this enhancement 54

4.10 Profile of a scan line from the visible portion of the Airborne Scanner data (Data Set 4), top, and the Landsat TM data (Data Set 8), bottom. Scan line was taken across forest cover types (left) and grassland cover types (right). The change from forest to grass is identified by the arrowhead. . . . 86

4.11 Profile of a scan line from the near-infrared portion of the Airborne Scanner data (Data Set 4), top, and the Landsat TM data (Data Set 8), bottom. Scan line was taken across forest cover types (left) and grassland cover types (right). The change from forest to grass is identified by the arrowhead. . . . 87

4.12 Profile of a scan line from the middle-infrared portion of the Airborne Scanner data (Data Set 4), top, and the Landsat TM data (Data Set 8), bottom. Scan line was taken across forest cover types (left) and grassland cover types (right). The change from forest to grass is identified by the arrowhead. . . . 88

4.13 Photographic reproduction of a portion of Study Area 3 from Geoscan's MKII Airborne Multispectral Scanner. The black line marks the location of the scan line profiles taken from this area 89

INTRODUCTION

1.1 OVERVIEW

The security of the United States of America depends on a military that is able to fight and win in all types of environments and conditions. This requires regular training of personnel in geographic areas that simulate future battlefields. Many of these training areas are located in arid or semi-arid regions of the world. As such, they are environmentally sensitive and require special management practices to ensure their continued use.

The United States Army Construction Engineering Research Laboratory (USACERL) has developed a method of monitoring changes in land condition on training areas throughout the world. The Integrated Training Area Management program was designed to provide land managers with necessary information to ensure these areas are not destroyed by overuse.

The Land Condition-Trend Analysis (LCTA) program is a major part of the ITAM program. The LCTA program is a way of obtaining very detailed information about the condition of military training lands. A report by Diersing et al. (1989) outlines the primary objectives of this program, which are to evaluate and monitor the capability of the land to meet multiple-use demands, to include military training, on a

sustained basis. When changes occur such that the available resources are endangered, this program gives the land manager a decision base for altering land management practices to ensure long-term resource availability. This program also standardizes the data collecting and reporting methods on an Army-wide level.

Multiple-use is defined by Section 601 of the Federal Land Policy and Management Act (U.S. Congress, 1976) as:

> ...a combination of balanced and diverse resource uses that takes into account the long-term needs of future generations for renewable and nonrenewable resources, including, but not limited to, recreation, range, timber, minerals, watershed, wildlife and fish, and natural scenic, scientific and historical values; and harmonious and coordinated management of the various resources without permanent impairment of the productivity of the land and the quality of the environment...

Remote Sensing technology is utilized initially in the process of selecting permanent plots within military installations. For this application, a satellite image is processed to identify areas that are spectrally homogeneous based on reflectance values in the green, red and near infrared wavelength bands. The resulting image is subsequently superimposed on a digital soil data layer within a geographic information system (GIS). Areas that have homogeneous soil and land cover are identified as possible locations for the LCTA plots. These plots are established on a stratified-random basis, that is, the number of plots assigned for each land cover and soil category is proportional to the percent of land area that it occupies.

Although remote sensing technology is used extensively to identify possible locations for permanent LCTA plots, a very limited amount of remote sensing research is presently being conducted to assess land condition changes in conjunction with the LCTA plots. Remotely sensed data will not replace the need for detailed ground reference data within the LCTA plots on military installations. However, it may provide the land manager with an improved overall estimate of land conditions to enable him or her to better manage the Army's need for training and the land's capacity to support that training.

While the information collected under the LCTA program is very valuable, it is also very labor intensive. According to Diersing et al. (1989), field crews gather information on areas or plots that measure 6 x 100 meters. General guidelines suggest that one plot be designated for every 200 hectares (500 acres). The proportion of the training area that would be covered by plots following these guidelines represents only 0.03% of the training area. Since the number of possible plots for large training areas could conceivably become unmanageable, the maximum number of plots for a particular installation is limited to 200. This information consists of topographic features, soil characteristics, climatic variables, wildlife species, surface disturbance, percentage of bare ground, gravel, rock, duff, litter and basal cover. These plots are visited annually to determine changes that have occurred, and a detailed reconnaissance for each plot as outlined above is conducted every three years.

Pinon Canyon Maneuver Site (hereafter referred to as Pinon Canyon) is a military training area located in Southeastern Colorado. It is one of several military installations where the Integrated Training Area Management program is in effect. As such, several LCTA plots have been identified and inventoried over a period of several years. A concentrated effort is being made in this area to ensure that the land can meet the training needs of the Army both now and in the future.

This research was divided into two major categories. The first focused on the ability of several types of remotely sensed data having different spatial resolutions to detect damage caused by off-road vehicular traffic, primarily military tracked vehicles, on portions of training areas located within Pinon Canyon. This damage is hereafter referred to as "tank trails." The second portion of this research involved the comparison of classification accuracies of two data sets having different spatial resolutions. A per-point classifier was used for the classification.

The techniques used in this research to detect tank trails are very likely applicable to any agency interested in monitoring off-road vehicular damage in an arid or semi-arid environment. Several studies in the past have concentrated on the detrimental effects of recreational off-road vehicular traffic to plant and animal communities and the surrounding environment. In these areas soil is compacted, vegetation is lost, and erosion rates increase. The effects of off-road

vehicular travel and subsequent damage to the environment can literally last for decades (Prose 1985). Very little research has been conducted, however, to determine the ability of various types of remote sensor data to detect this damage.

1.2 OBJECTIVES

The primary objective of this research was to determine the capabilities and limitations of remote sensor systems having different spatial resolutions to aid in monitoring U.S. Army training maneuver sites. This was accomplished in two phases. First, the ability of these systems to detect off-road tracked vehicular damage on military installations was evaluated. Second, two different types of remotely sensed data having different spatial characteristics were evaluated to assess their effectiveness for per-point classification on different vegetative cover types. The following sub-objectives were identified:

i) Evaluate several edge and line enhancement methods or techniques to determine their effectiveness in enhancing tank trails. (For clarity, all methods or techniques are hereafter referred to as enhancement techniques). These enhancement techniques included high-pass and low-pass filters, Laplacian, Sobel, Roberts, Mero-Vassy, Prewitt, Kirsch, and Chittineni edge detectors, and directional line filters. A "running difference" or derivative technique, and an isogradient technique were also tested.

ii) Identify the optimum digital filter or enhancement technique to use for enhancement of tank trails in digital data.

iii) Evaluate the ability of sensor systems with different spatial resolutions to detect tank trails in digital data.

iv) Assess the impact of spatial resolution on classification performance of different vegetative cover types when using a per-point classifier.

v) Assess the interrelationships between sensor spatial resolution and the spatial characteristics of forest and rangeland cover types.

LITERATURE REVIEW

2.1 EFFECTS OF OFF-ROAD VEHICULAR TRAVEL

Several studies in the past have shown the detrimental effects of off-road vehicle use on natural ecosystems. These areas lose natural vegetation, the soil becomes compacted, and erosion increases (Green et al., 1973; Wilshire, 1977; Goodwin, 1977; Iverson et al., 1981; Goran et al., 1983; Webb and Wilshire, 1983; Wilshire, 1984; Tuttle and Griggs, 1987; Shaw and Diersing, 1990). Prose (1985) has shown that the effects of military tracked vehicle maneuvers in a semi-arid environment can last for decades.

Army Regulation AR 200-2 requires that long-term impacts on natural resources caused by military training activities be reduced or avoided (Prose, 1985). There are methods currently in place to aid land managers in monitoring U.S. Army training areas. The Integrated Training Area Management (ITAM) program was implemented by the U.S. Army in 1987 to ensure that the training areas are not ruined through overuse. It has been estimated that a savings of $5.00 to $27.00 in rehabilitation costs will be saved for every dollar spent on the ITAM program (Diersing et al., 1989).

The Land Condition Trend Analysis (LCTA) program is the sub-program within ITAM through which monitoring of the land

is accomplished. Shaw and Diersing (1989) have shown that this is an effective tool in monitoring U.S. Army training areas. Guidelines to minimize damage caused by military tracked vehicles have been established as a direct result of these programs (Diersing et al., 1988; Shaw and Diersing, 1989).

2.2 REMOTE SENSING AND OFF-ROAD VEHICULAR TRAVEL

Remote sensing technology as an aid in monitoring land conditions at military installations located in semi-arid regions has had limited use in the past. In an unpublished report, Ribanszky et al. (1990) describe the successful use of SPOT multi-spectral data in detecting land cover changes within U.S. Army training lands. This is accomplished by converting the SPOT digital data to a normalized difference vegetation index (NDVI). This research, however, is in Hohenfels, Germany, which is not considered a semi-arid region.

Warren and Hutchinson (1984) describe the use of remote sensing in an arid environment to evaluate different environmental variables as indicators of rangeland change. In this study, disturbance was related to changes in overall vegetation density and the ratio between shrubs and grasses. Other studies have documented the use of remote sensing technology in monitoring arid and semi-arid regions (Peterson et al., 1987; Johnson et al., 1989; Teuller, 1989).

Graetz and Pech (1987) have shown the advantages of using both Landsat Thematic Mapper (TM) and aerial photography for assessing the human impacts of oil exploration in an arid environment. The coarse resolution of Landsat TM limits its ability to detect small linear features such as seismic exploration tracks, but the repetitive and large-area coverage make it very useful for detecting 'problem' areas. Large-scale photography (1:2,000 - 1:10,000) was best for evaluating processes of erosion along these tracks, and subsequent revegetation. The high cost and restrictive coverage, however, are the disadvantages of using aerial photography for monitoring desert landscapes.

2.3 EDGE AND LINE ENHANCEMENT TECHNIQUES

The use of different techniques to enhance edge and linear features in remotely sensed digital data has received much attention in previous years (Weszka and Eberlein, 1975; Robinson, 1977; Vanderbrug, 1976; Chavez and Bauer, 1982; Chittineni, 1982; Ford et al., 1983; Gil et al., 1983; Sullivan et al., 1984; Lenz, 1987; Chen and Tsai, 1988; Berthod and Serendero, 1988; Krahe and Pousset, 1988; Kundu, 1989). Linear features may include many things from geologic lineaments caused by joints and faults or other natural phenomena, to the ridges and valleys on fingers that create fingerprints (Verma et al., 1987; Peters et al., 1988).

Several papers provide a survey of different types of edge and line detectors, and give a brief explanation of each

(Davis, 1975; Shaw, 1979; Peli and Malah, 1982). Edge detection may be divided into two major groups: local and regional. Local edge detectors usually employ small windows that move throughout the imagery. These windows are usually 3 x 3 or 5 x 5, and can be thought of as differential operators. That is, they detect differences between brightness values of neighboring pixels and thus define "edginess" at each point in the image. Regional operators, as the name implies, cover areas much larger than the edges to be detected. These operators are designed to detect edges of varying widths between two large areas, each having unique and somewhat constant brightness values (Shaw, 1979).

Local edge detectors may be subdivided into two types: linear and nonlinear (Rosenfeld and Kak, 1976; Peli and Malah, 1982; Jensen, 1986). Linear edge detectors are performed using linear combinations of pixels, e.g., adding, subtracting, multiplying or dividing pixel values within digital imagery. Nonlinear edge detectors, however, are performed using nonlinear combinations of pixels, e.g., performing exponential or logarithmic functions on pixel values (Jensen, 1986).

2.3.1 LINEAR EDGE DETECTION TECHNIQUES

A high-emphasis spatial frequency filter, or high-pass filter is one method of linear edge detection (Davis, 1974). Sharp changes in brightness values throughout an image (i.e., the presence of edges or lines) will be amplified by a high-

pass filter. Sullivan et al. (1984) and Jensen (1986) discuss the use of low-frequency or low-pass filters. These types of filters tend to suppress much of the "salt and pepper" noise that is present in many digital images.

A simple and yet very effective technique for detecting lines and edges is a running difference or gradient (first derivative) technique (Rosenfeld and Kak, 1976; Hord, 1982; Jensen, 1986). It is often referred to as a first derivative operator because changes in brightness value over a standard unit of one pixel are measured. This technique is performed by subtracting each pixel in the image from its immediate neighbor. A subtraction of pixels in the vertical direction enhance horizontal lines and edges. Similarly, a subtraction of pixels in the horizontal direction enhance vertical lines and edges. In areas where no difference in brightness value occur (i.e., the values of adjacent pixels are equal), the result is zero. These areas of little or no change are assigned a gray tone. If a negative value occurs, the pixel is assigned a darker tone. Conversely, if a positive value occurs, the pixel is assigned a lighter tone. Thus, a band of dark and light toned pixels surround all linear features and edges (Jensen, 1986). The visual effect of this procedure is an apparent 3-dimensional image, with the bands of dark and light pixels forming lines in the image that appear to be depressed or raised on the image, based on which direction the image was shifted.

For the gradient image, if pixels in the y direction are subtracted from each other, lines and edges oriented in the x direction are enhanced. This logic holds true for other directions as well.

An operator similar to the gradient technique was first proposed by Roberts (1965), and is mentioned in works by Duda and Hart (1973), Davis (1974), Peli and Malah (1982) and Jensen (1986). This operator will detect either a horizontal or vertical edge. It uses a 2 x 2 window as follows:

i,j	i,j+1
i+1,j	i+1,j+1

(In cases of 2n x 2n filters (i.e., 2 x 2, 4 x 4, etc.), the location of the output is assigned to the upper left cell). The formula that the Robert's operator uses in calculating the filtered image is as follows:

Image = [abs((i,j) - (i+1,j+1)) + abs((i,j+1) - (i+1,j))]

where abs refers to absolute value.

Rosenfeld and Kak (1976) discuss in great detail a very useful class of linear filters known as the Laplacians. These filters are isotropic second derivative operators, and are rotation invariant (Duda and Hart, 1973). That is, rotating the filter by rearranging the coefficients will not change the output. Since they are isotropic second derivative operators, lines and edges in all directions are simultaneously enhanced using this technique. A very basic Laplacian digital filter

is defined by the following 3 x 3 window (Rosenfeld and Kak, 1976):

0	-1	0
-1	4	-1
0	-1	0

The numbers in this filter and the filters that follow act as multiplicative coefficients. The cells are then averaged, and the resulting value is assigned to the location that coincides with the center cell of the window. Different coefficients may be placed in these filters to enhance specific features of interest. For example, Rosenfeld and Kak (1976) and Jensen (1986) suggest experimenting with different coefficients interactively until the desired product is obtained. Robinson (1976) and Sullivan et al. (1984) indicate that a filter with two non-zero coefficients in the 8 cells surrounding the center cell is referred to as a bi-Laplacian filter.

Rosenfeld and Kak (1976) compared images created using the gradient function to images created using Laplacian filters. They found that the gradient images generally produced better results for edge detection. They also showed that the Laplacian filters were usually better for detecting lines than was the gradient method. In direct contrast to these findings, Hord (1982) indicated that the gradient was usually preferred for finding lines, whereas the Laplacian filters were more useful in edge and boundary detection.

Previous studies have documented the value of filters designed to enhance lines and edges of a specific orientation. (Vanderbrug, 1976; Robinson, 1977; Chittineni, 1983; Sullivan, et al., 1984). These filters generally are constructed with zero weighting (i.e., the sum of coefficients in the filter equal zero) so that no output is produced over areas that have no edges or lines present (Jensen, 1986).

Robinson (1977) provides a number of directional line filters that were first described by Prewitt (1970) and Kirsch (1971) as "compass gradient masks." In this case, the word masks is used as a synonym for filters. These types of filters are useful for applications that require edges and lines of a particular orientation to be enhanced. When an application requires that all edges and lines be enhanced regardless of orientation, however, a single filter will not provide sufficient information.

2.3.2 NONLINEAR EDGE DETECTION TECHNIQUES

Several nonlinear enhancement techniques have been proposed. A simple nonlinear enhancement technique for edge and line detection was suggested by Hord (1982). He developed a way to avoid loss of detail in certain directions when using the simple gradient technique. The directional derivative in the x direction may be represented as dG/dx. Similarly, the difference in the y direction (y directional derivative) may be represented as dG/dy. The isotropic first derivative, or gradient, is then found according to the following equation:

$$\text{Image} = [(dG/dx)^2 + (dG/dy)^2]^{1/2}$$

This technique produces an image that is very similar to the regular gradient image. The advantage is that lines and edges in all directions are enhanced.

The Sobel operator, as described by Duda and Hart (1973), Robinson (1976), Rosenfeld and Kak (1976) and Jensen (1986), is also a nonlinear operator. This operator is analogous to a combination of two compass gradient masks as described earlier, namely the North and East directions (Robinson 1977). The two masks that are combined are as follows:

X Component:

-1	0	1
-2	0	2
-1	0	1

Y Component:

1	2	1
0	0	0
-1	-2	-1

A new image is created out of the combination of the X and Y components as follows:

$$\text{Image} = (X^2 + Y^2)^{1/2}$$

where X and Y are the images created by applying each respective filter to the original image. The coefficients 1, 2, and 1 are based entirely on intuitive grounds (Duda and Hart, 1973). Nevertheless, Jensen (1986) found that the Sobel operator worked very well on a set of thermal-infrared data obtained over a portion of the Savannah River.

An operator that uses the same principle as the Sobel operator was suggested by Mero and Vassy (1975) and described by Shaw (1977). Two filters are again used: one that enhances edges and lines oriented in the y direction, and another that

enhances those oriented in the x direction. The advantage of the Mero-Vassy operator is computational efficiency. This operator consists of 2 x 2 windows as follows:

-1	1
-1	1

1	1
-1	-1

In order to perform the Mero-Vassy filters with systems restricted to 3 x 3 windows, the coefficients for the center rows and columns are set to zero.

There are many techniques and filters available that will enhance edges and lines in remote sensor data. This discussion has dealt with relatively small window sizes (2 x 2, 3 x 3, etc.). There are, however, techniques that use larger windows, depending on the intended application. A compromise must be found regarding window size. A very small window will enhance many fine details, but will also be very sensitive to digital "noise." A larger window is less sensitive to noise, but tends to subdue the fine details required for some applications (Davis, 1974). The analyst must interactively select the combination that best enhances the imagery for his or her application requirements.

2.4 SPATIAL RESOLUTION CONSIDERATIONS

The ability of a sensor to detect certain features on the ground is a function of several things. First, the spatial resolution of a sensor will greatly influence which objects on

the ground are detected. Spatial resolution refers to how small an object can be on the ground and still be detected by the sensor system (Lillesand and Kiefer, 1987). Jensen (1986) defines spatial resolution as "the smallest angular or linear separation between two objects than can be resolved by the sensor."

Spatial resolution is closely related to the instantaneous field of view (IFOV) of the sensor system involved. The IFOV refers to the area on the ground from which information is received by one ground resolution element and subsequently assigned to one pixel in remotely sensed digital imagery. Because IFOV is often the limiting factor determining the ability of a sensor to discriminate between two objects on the ground, the IFOV is often referred to as the spatial resolution of the sensor. Therefore, for purposes of this research, the IFOV of a sensor system will hereafter be referred to as the spatial resolution of the sensor.

Second, the amount of contrast between an object and its surrounding environment will also influence the detectability of that object. For instance, a concrete road of high reflectance may not be detectable in Landsat TM imagery with a 28.5 meter spatial resolution (28.5 meters on each side of a pixel) if that road occurs in an urban environment where most of its surroundings are composed of concrete structures. However, a bridge of similar spectral characteristics that spans a water body will be easily detected because of the spectral contrast between the bridge and the water.

2.5 SPATIAL RESOLUTION AND CLASSIFICATION ACCURACY

Several studies in previous years have investigated the effect of spatial resolution of the sensor system involved on classification accuracy and area mensuration using automated information extraction techniques (Simonett and Coiner, 1973; Kan et al., 1975; Thomson et al., 1975; Clark and Bryant, 1977; Sadowski et al., 1977; Latty and Hoffer, 1981; Hoffer et al., 1982; Acevedo et al., 1984; Irons et al., 1984; Williams et al., 1984; Latty et al., 1985; Irons and Kennard, 1986; Woodcock and Strahler, 1987; Benjamin and Gaydos, 1990).

Schwarz et al. (1969), as related by Simonett and Coiner (1973), have documented a point that is important in understanding the relationship between sensor spatial resolution and informational content. They indicate that large homogeneous areas that contain a single informational category may effectively be imaged with coarse resolution. However, complex, finer-scale environments will require a finer spatial resolution so that a greater proportion of the pixels present will contain information from a single informational class, rather than from multiple categories.

Several studies have focused on the classification accuracy of a single, apparently homogeneous informational class: a forest canopy (Kan et al., 1975; Sadowski et al., 1977; Latty and Hoffer, 1981). They have found that as spatial resolution increases (becomes finer), spectral variance increases, thus reducing the separability or

interspersion of spectral clusters in feature space. The result is a paradox: higher (finer) spatial resolution sensors tend to produce lower classification accuracies in forest cover types. This is, in part, due to the shadow effects and spectral variation within a forest canopy on and between individual tree crowns (Hoffer, 1982). Latty and Hoffer (1981) found that classification accuracies for classes with lower spectral variability (e.g., crop, pasture, soil) did not significantly change with increased spatial resolution.

During a systems study to analyze the optimal spatial resolution for Landsat Thematic Mapper, Thomson and Erickson (1975) classified an agricultural environment of low spectral variability using digital data that simulated sensor systems having IFOV's of 30 and 60 meters, respectively. They found no significant differences in these classification accuracies, which is consistent with earlier studies. Markham and Townshend (1981) observed similar results over several cover types in eastern Maryland with a data set that was progressively degraded to 10, 20, 40 and 80 meter spatial resolution. They also found that the influence of spectral variability on classification accuracy is affected by the location of spectral clusters in feature space. They found that it was impossible to predict the results of a classification solely on spectral variability and the category type.

Several studies have documented the effects of boundary pixels on classification accuracy. Morgenstern et al. (1977)

found that a higher relative frequency of boundary pixels in the coarse spatial resolution data (50 meter to 80 meter) tended to decrease the accuracy of agricultural crop mensuration. Landgrebe et al. (1977) found that although classification accuracy improved slightly with lower spatial resolution data, the decrease in area mensuration accuracy was larger than the improved classification accuracy. Markham and Townshend (1981) indicated that boundary pixels in the lower spatial resolution data tended to decrease accuracy for classes containing small features such as roads and small water bodies. They also indicated that boundary pixel and scene noise effects may offset each other, thus keeping classification accuracies relatively unchanged for several different resolutions.

Clark and Bryant (1977) observed an increase in classification accuracy in urban categories as spatial resolution was degraded from 7.5 meters to 60 meters. Badhwar et al. (1984) and Haack et al. (1987) indicate that Landsat MSS with 80 meter resolution produces better classification results than Landsat TM in complex environments such as urban or near-urban land use categories. They point out, however, that Landsat TM is superior to Landsat MSS in delineating boundaries due to the higher spatial resolution.

Other studies have also shown that high spatial resolution is preferred over lower resolutions for certain applications (Parks et al., 1987; Curran and Williamson, 1988; Benjamin and Gaydos, 1990). Parks et al. (1987) found that

finer resolution Landsat TM and SPOT MSS were better able to delineate vegetation and other surface features in spatially and spectrally complex coal surface mines. Curran and Williamson (1988) found that a spatial resolution of 2 meters and 5 meters was best for estimating the per-field green leaf area index (GLAI). Benjamin and Gaydos (1990) found that a spatial resolution of 3 meters was best for extracting road features from scanned aerial photography.

2.6 DATA COMPRESSION THROUGH PRINCIPAL COMPONENTS ANALYSIS

A procedure known as a principal components transformation is a commonly used procedure to extract the maximum amount of information from the bands and at the same time, to reduce the dimensionality of remote sensor data, particularly multispectral scanner data. To better understand the transformation, imagine two multispectral bands, X and Y. A two-dimensional plot of these bands would be two orthogonal axes with the origin at (X,Y) location (0,0). If the brightness values of all pixels in these two bands were plotted, the result would appear to be an ellipse. The maximum amount of variability in these pixels would probably not coincide with either of the two orthogonal axes, and the mean of these pixels would probably not be exactly at the origin, (0,0).

The transformation actually occurs by transforming or reprojecting the origin of this set of axes to the location of the means for both bands. The axes are then rotated so that

one of the axes coincides with the maximum amount of variance within the conceptual ellipse. The axis that coincides with the maximum amount of variance within the ellipse is the first principal component of the spectral bands and contains most of the information available in these spectral bands. The axis that is perpendicular to the first principal component is the second principal component. It contains a smaller amount of information (i.e., variance) than the first principal component, but is still valuable. The first three principal components in a multispectral data set such as Landsat TM will often contain 95 to 98% of the total variance or information content. Therefore, this is an efficient way to reduce the dimensionality of a large multispectral data set (Jensen 1986).

2.7 SELECTIVE PRINCIPAL COMPONENTS ANALYSIS

Chavez and Kwarteng (1989) have recently introduced a procedure known as the selective principal components analysis. This procedure compresses the data within each portion of the electromagnetic spectrum (i.e., visible, near-infrared, middle-infrared) into one band. The resulting data set for Landsat TM reflective data will thus contain three bands. Band 1 is the first principal component of the visible bands, band 2 is the first principal component of the near-infrared band, and band 3 is the first principal component of the middle-infrared bands. This procedure assures that most of the information of interest is incorporated into the first

component from each region of the electromagnetic spectrum. This technique also enables easier interpretation of the compressed data as compared to a principal components analysis utilizing a combination of all bands from all regions of the spectrum.

In summary, much work has been done in recent years to determine techniques that best enhance lines and edges in remote sensor data. There are, however, dramatic differences in the results obtained by different authors. As previously mentioned, Rosenfeld and Kak (1976) found that the Laplacian filters were usually better than gradient images for detecting lines. Hord (1982), however, documented that the gradient images were better than Laplacian filters for lines. Therefore, because there is no clear indication in the literature of the best technique to use for enhancing linear features in digital remote sensor data, a large portion of the current research was focused on the comparison of line and edge enhancement techniques to determine which is best for enhancing tank trails. In addition, because there have been relatively few studies documenting the relationship of classification accuracy as a function of remote sensor spatial resolution and cover type, the balance of the current research was focused on classification accuracy as a function of sensor spatial resolution versus cover type involved.

METHODS AND MATERIALS

3.1 STUDY AREAS

Pinon Canyon is located in Southeastern Colorado. It was obtained by the U.S. Army in 1983 to conduct military training maneuvers which commenced in 1985 and have continued to the present. Figure 3.1 shows the location of Pinon Canyon and the three study areas that were used in this research. Each study area is approximately 45 square kilometers, and are portions of different training areas within Pinon Canyon.

Study Area 1 is a portion of a military training site on which military training units have not been allowed to train since January 1989. Study Area 2 is a portion of a training site on which maneuvers were conducted since January 1989. A major military exercise was being conducted in this region at the time the multispectral data set was acquired (July 13-15, 1989).

The majority of Study Area 3 covers portions of a protected site within Pinon Canyon. Because of steep slopes and thin soils, military training is not conducted in this region. Area 3 also covers locations that are outside the boundary of Pinon Canyon (northern part of imagery), and sites that are available to military units for training (southern part of imagery).

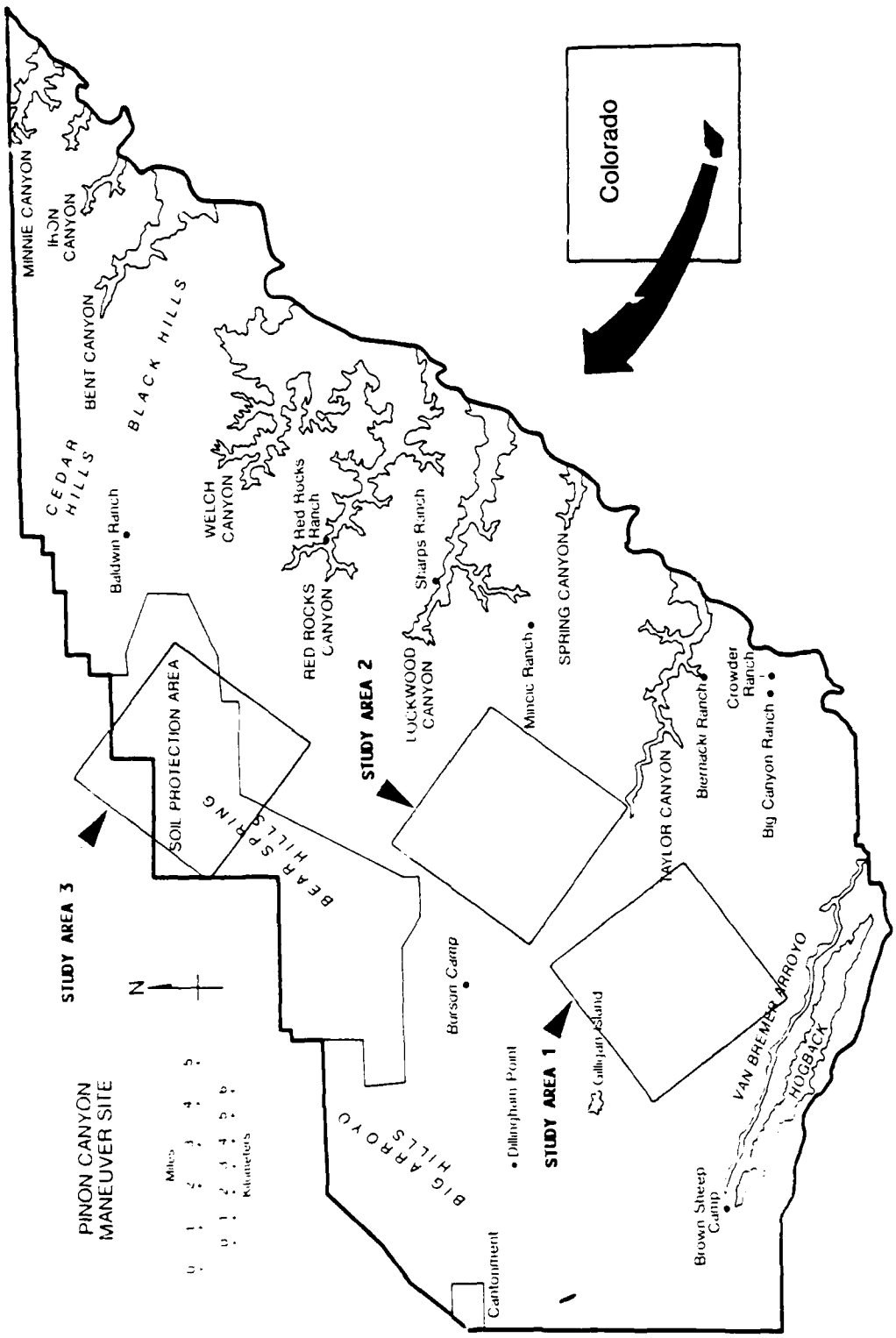

Figure 3.1. Location of Pinon Canyon Maneuver Site and selected study areas. (After Shaw et al., 1989)

3.2 DATA USED

The U.S. Army Cold Regions Research Engineering Laboratory (USACRREL) has obtained several types of remotely sensed data for Pinon Canyon. The data used in this research (Table 3.1) included aerial photography obtained under the National Aerial Photography Program (NAPP) and the National High Altitude Photography (NHAP) program. Imagery from Geoscan's MkII Airborne Multispectral Scanner (AMSS) was also available (Geoscan Pty. Ltd.). It is capable of obtaining information in 24 spectral channels. This imagery consisted of portions of three different flight lines flown over Pinon Canyon on the same day. Additionally, imagery from the French SPOT satellite and Landsat Thematic Mapper (TM) were analyzed. A combination of SPOT Panchromatic and Landsat TM was created using the Intensity, Hue, Saturation transformation and used as an additional data set. Unless otherwise indicated, all data, except the SPOT Panchromatic imagery, is hereafter referred to as the "multispectral data set."[1] In cases where only selected data are used, they are referred to by their specific data code designator as found on Table 3.1.

Figure 3.2 graphically shows the relationship of spectral bands for Data Sets 4, 6, and 8. It is obvious from this figure that the band widths of Geoscan's MKII Airborne

---

[1]Although aerial photography is not normally referred to as "multispectral", different portions of the spectrum comprise the information in color infrared photography. For purposes of this research, therefore, it is included in the "multispectral data set."

Table 3.1. Pertinent information concerning remote sensor data used in this research.*

DATA CODE DESIGNATOR	SENSOR	TYPE OF DATA	ACQUISITION DATE	SCALE/RESOLUTION
1	Aerial Photography	NAPP Color IR	September 1988	1:40,000 1.25 meter resolution
2	Aerial Photography	NHAP Color IR	October 1983	1:58,000 1.81 meter resolution
3	Digitized Aerial Photography	NAPP Color IR (Enlarged)	September 1988	Digitized to (approx) 5 meter resolution
4	Airborne Multispectral Scanner	24-Channel Multispectral	15 July 1989	Resampled to (approx) 6.5 meter resolution
5	Digitized Aerial Photography	NAPP Color IR (Original)	September 1988	Digitized to (approx) 8 meter resolution
6	SPOT Satellite	Panchromatic	13 July 1989	10 meter resolution
7	IHS Transformation	Combined SPOT/TM	13/15 July 1989	Resampled to 10 meter resolution
8	Landsat Thematic Mapper	7-Band Multispectral	15 July 1989	Resampled to 25 meter resolution

* Ordered according to spatial resolution (1 = highest resolution).

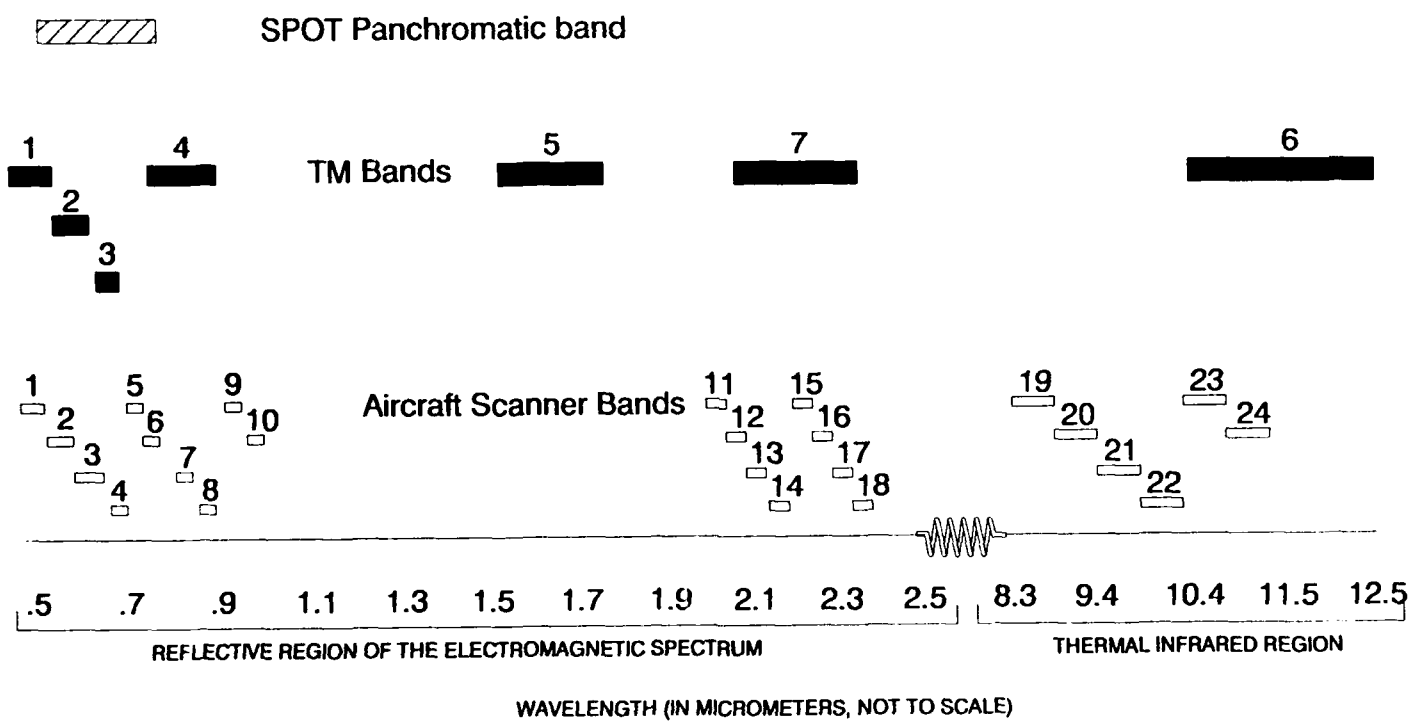

Figure 3.2. Spectral band comparison between SPOT Panchromatic, Landsat Thematic Mapper and Geoscan's MKII Airborne Multispectral Scanner.

Multispectral Scanner are very narrow and closely spaced. Table 3.2 contains the actual band widths and ranges for each of the 24 channels of Data Set 4.

Table 3.2. Geoscan's MKII Airborne Multispectral Scanner (AMSS) Band Specifications.

REGION	BAND NUMBER	BAND WIDTH (μm)	RANGE (μm)
VISIBLE	1	.042	.5010 - .5430
	2	.067	.5495 - .6165
	3	.071	.6095 - .6805
	4	.024	.6810 - .7050
	5	.024	.7050 - .7290
NEAR IR	6	.023	.7285 - .7515
	7	.022	.8190 - .8410
	8	.022	.8620 - .8840
	9	.021	.9045 - .9255
	10	.020	.9450 - .9650
MIDDLE IR	11	.044	2.0220 - 2.0660
	12	.044	2.0660 - 2.1100
	13	.044	2.1140 - 2.1580
	14	.044	2.1540 - 2.1980
	15	.044	2.1980 - 2.2420
	16	.044	2.2420 - 2.2860
	17	.044	2.2860 - 2.3300
	18	.044	2.3300 - 2.3740
THERMAL IR	19	.530	8.3750 - 8.9050
	20	.530	8.9050 - 9.4350
	21	.530	9.4350 - 9.9650
	22	.533	9.9535 -10.4865
	23	.533	10.4835 -11.0165
	24	.533	11.0135 -11.5465

Preprocessing of Data Sets 4 and 8 included fixing bad scan lines in Data Set 4, and masking clouds and cloud shadows out of both data sets. Additionally, a selective principal components analysis was performed on both data sets to reduce the dimensionality of the data (Chavez and Kwarteng, 1989).

Ground truth information for this research consisted of aerial photography (as discussed above). Detailed information collected by field crews from Fort Carson, Colorado and Colorado State University during the summer of 1989 was also available from several LCTA plots located within each study area (Appendix 1). This data included information such as the amount of bare ground, gravel, rock, duff, litter and basal cover located at each plot. Additionally, field work was conducted by the author over many portions of the study areas to determine major vegetative cover types and approximate percent ground cover.

3.3 DETECTION OF OFF-ROAD VEHICULAR DAMAGE

The first specific sub-objectives defined for this research were to evaluate several line and edge detectors, define the optimum filter for enhancing tank trails, and evaluate the effectiveness of different sensor systems for detecting these trails. Berthod and Serendero (1988) describe three types of lines that can be found in satellite imagery. They are, (1) thick lines that have two nonparallel edges, (2) thin lines approximately one pixel wide, and (3) "virtual" or inferred lines. An example of the last type are small lanes between fields, etc. Although all lines were enhanced using various line and edge detectors, this research was primarily focused on lines of the first and especially the second type.

A three-phase evaluation was used to determine which enhancement techniques and data sets most effectively enhanced

tank trails. A distinction must be made between the terms enhancement technique and filter. Enhancement technique refers to a method for enhancing certain features (i.e., tank trails) such as Laplacian, high-pass and gradient, etc. Filter, on the other hand, refers to the specific window into which different coefficients are placed to perform a specific function such as smoothing the data or enhancing lines or edges. For the first phase of this evaluation process, several filters having different coefficients for each technique (see Appendix 3) were applied to a portion of Study Area 2 to determine an optimal filter within each technique. (This resulted in a combination of twenty enhancement technique/filter combinations which are described in Section 3.3.2). Second, after the best enhancement technique/filter combinations were identified, all twenty combinations were applied to a portion of Study Area 1 to determine which technique best enhanced tank trails for each of the nine data sets that are described below. Third, after an optimum technique was determined for each data set, the best enhanced image from each data set was compared to the best enhanced image from other data sets to determine which combination of remote sensor data and enhancement technique is best able to detect tank trails.

3.3.1 DATA USED FOR DETECTION OF TANK TRAILS

The entire multispectral data set (less the NHAP photography that was obtained before any military tracked

vehicles trained in the area), as well as the SPOT Panchromatic data set were used for this portion of the research. Additionally, a one-band image from each data set, (the middle-infrared component where available), was used to assess whether a black and white image (1 band) or color composite image (3 bands) produced better results using these methods. The single band from aerial photography was obtained by using the red portion of the red, green, blue (RGB) video digitized data which represents the photographically sensitive near-infrared portion of the spectrum.

When the original aerial photography was video digitized, several fine details were lost due to the screen resolution of the monitor or video camera. Therefore, an additional data set was created from NAPP aerial photography by enlarging the test portion of Study Area 1 to twice the original size. This portion was again video digitized. A one-band image was again created from the red portion of the RGB digitized data.

A total of nine data sets were thus used from Study Area 1 to evaluate different enhancement techniques. These data sets are similar to those found in Table 1 with the exception that one-band and three-band data sets are now included. These nine data sets were (ordered according to descending spatial resolution): (1) An enlarged photograph of NAPP aerial photography, one band, (2) Digitized NAPP photography, one band, (3) Digitized NAPP photography, three bands, (4) Aircraft Multispectral Scanner, one band, (5) Aircraft Multispectral Scanner, three bands, (6) SPOT Panchromatic

imagery, (7) SPOT/TM intensity, hue, saturation transformation, (8) Landsat Thematic Mapper, one band, and (9) Landsat Thematic Mapper, three bands.

3.3.2 IMAGE ENHANCEMENT TECHNIQUES

The first phase of the evaluation of enhancement techniques and filters was conducted using a portion of Study Area 2 of Data Set 4. This established a set of enhancement techniques that satisfactorily enhanced tank trails. The middle-infrared band of this imagery was used for this initial phase of the research because of the high spectral response of soil in this portion of the electromagnetic spectrum.

Several techniques were tested for their effectiveness in enhancing off-road vehicular damage. These techniques included high-pass and low-pass filters, edge and line detectors such as Laplacian (weighted and zero-weighted), Sobel, Roberts, Mero-Vassy, Prewitt, Kirsch, and Chittineni line and edge detectors. Directional line filters that enhance lines in a particular direction were tested. A running difference or gradient technique, and an isogradient technique were also evaluated to determine which technique produced optimum results. Appendix 3 contains a complete list of techniques attempted, coefficients used, and also indicates the best filter from each category.

The following section contains a summary from Appendix 3 of the best techniques and filters that were applied to Study Area 1. Table 3.3 gives a summary of this information and the

data sets to which they were applied. Each cell in this matrix represents one processed image (i.e., a total of 180 images were created for evaluation). The characteristics of the 20 different enhancement techniques used, as listed in Table 3.3 are as follows:

1. Laplacian, no weight.

0	-1.75	0
-1.75	7	-1.75
0	-1.75	0

2 and 3. Laplacian, weighted.

0	-1	0
-1	5	-1
0	-1	0

1	-2	1
-2	5	-2
1	-2	1

4. Sobel edge enhancement. (Image = $(X^2 + Y^2)^{1/2}$.

X Component:

-1	0	1
-2	0	2
-1	0	1

Y Component:

1	2	1
0	0	0
-1	-2	-1

5. High-pass filter, 3 x 3 window.

-1	-1	-1
-1	9	-1
-1	-1	-1

6. Sobel edge enhancement, applied to the high-pass filtered image from number 5 above. (The same X and Y components from the regular Sobel image (above) were used for this technique).

Table 3.3. Matrix used in evaluating enhancement techniques for different remote sensor systems.

	Laplacian (No Wt)	Laplacian (Filter 2)	Laplacian (Filter 3)	Sobel	Laplacian (5x5, No Wt)	Sobel w/Hi-Pass (3x3)	High-Pass (5x5)	Compass Gradients	Mero-Vassy	Prewitt	Chittineni	Vertical Gradient	Horizontal Gradient	Diag. Gradient (NW-SE)	Diag. Gradient (NE-SW)	Vert. and Horiz. Combined	Diagonal (Combined)	All Gradients combined	Isogradient	Raw Image
Enlarged Photo (Digitized) One Band																				
Digitized Photo One Band																				
Digitized Photo Three Bands																				
Aircraft MSS One Band																				
Aircraft MSS Three Bands																				
SPOT 10M Panchromatic																				
SPOT/TM IHS Three Bands																				
Landsat TM One Band																				
Landsat TM Three Bands																				

7. 5 x 5 Laplacian filter, zero weight.

0	-1	-2	-1	0
-1	-2	-4	-2	-1
-2	-4	40	-4	-2
-1	-2	-4	-2	-1
0	-1	-2	-1	0

8. Prewitt directional filters, combined into one image by simple addition.

North:

1	1	1
1	-2	1
-1	-1	-1

Northeast:

1	1	1
-1	-2	1
-1	-1	1

East:

-1	1	1
-1	-2	1
-1	1	1

Southeast:

-1	-1	1
-1	-2	1
1	1	1

South:

-1	-1	-1
1	-2	1
1	1	1

Southwest:

1	-1	-1
1	-2	-1
1	1	1

West:

1	1	-1
1	-2	-1
1	1	-1

Northwest:

1	1	1
1	-2	-1
1	-1	-1

9. Mero-Vassy filter. (Image = (abs(A) + abs(B))), where abs refers to the absolute value.

A Component:

1	1
-1	-1

B Component:

-1	1
-1	1

10. Prewitt gradient filter. (Image = A + B).

A Component:

1	1	1
0	0	0
-1	-1	-1

B Component:

1	0	-1
1	0	-1
1	0	-1

11. Chittineni filter (Laplacian).

-1	2	-1
2	5	2
-1	2	-1

12-19. Consider the following matrix of pixels from a hypothetical image. Each cell in the matrix may be represented as follows (the letters A-I are for convenience in referring to the cells):

$DN_{i-1,j-1}$ (A)	$DN_{i-1,j}$ (B)	$DN_{i-1,j+1}$ (C)
$DN_{i,j-1}$ (D)	$DN_{i,j}$ (E)	$DN_{i,j+1}$ (F)
$DN_{i+1,j-1}$ (G)	$DN_{i+1,j}$ (H)	$DN_{i+1,j+1}$ (I)

12. A vertical difference (or gradient) image was obtained by applying the following equation to each pixel in the image:

$$DN_{i,j} - DN_{i-1,j} \quad (\text{or } E - B).$$

This procedure enhanced horizontal lines and edges in the imagery.

13. A horizontal difference (or gradient) image was obtained by performing the following equation to each pixel in the image:

$$DN_{i,j} - DN_{i,j+1} \quad (\text{or } E - F).$$

This procedure enhanced vertical lines and edges in the imagery.

14. A NW-SE (diagonal) difference (or gradient) image was obtained by performing the following equation to each pixel in the image:

$$DN_{i,j} - DN_{i-1,j-1} \quad (\text{or } E - A).$$

This procedure enhanced lines and edges oriented in a NE-SW direction.

15. A NE-SW (diagonal) difference (or gradient) image was obtained by performing the following equation to each pixel in the image:

$$DN_{i,j} - DN_{i-1,j+1} \quad (\text{or } E - C).$$

This procedure enhanced lines and edges oriented in a NW-SE direction.

16. Adding the vertical and horizontal gradient images together created an image with all horizontal and vertical lines and edges enhanced.

17. Adding the diagonal gradient images together created an image with all diagonal lines and edges enhanced.

18. Adding all gradient images together created an image with lines and edges in all directions enhanced.

19. Another method of enhancing both horizontal and vertical lines and edges is given by the following equation:

$$(vert^2 + horiz^2)^{1/2}$$

Where $vert^2$ is the vertical gradient image (E - B) squared, and $horiz^2$ is the horizontal difference image (E - F) squared.

20. In addition to the techniques outlined above, the original imagery was used as another data set to evaluate. This provided a way of evaluating whether or not the enhancement techniques outlined above improved the ability to visually detect off-road vehicular damage.

3.3.3 METHOD OF EVALUATION

The enhancement techniques outlined above were determined in the first phase of the evaluation. The second phase of the evaluation of enhancement techniques was conducted on a portion of Study Area 1 to determine which enhancement technique worked best for each particular data set. After this was completed, the third phase of the evaluation compared the best enhanced image from each data set to the best enhanced image from other data sets.

The second phase of the evaluation determined the best enhancement technique (for enhancing tank trails) for each data set. This was determined by displaying two images simultaneously that were enhanced using the different techniques. The best of the two images were unanimously selected by a group of three analysts. Criteria used in selecting the best image was as follows: "Which image...(1)

is easier to visually interpret, (2) has the most contrast between the tank trail and background areas, (3) maximizes fine detail, such as tank trails, and (4) is best for overall interpretability?" The best image of the two was then retained on the display screen and the next image was displayed in place of the discarded image. These two images were then evaluated in a similar manner. This process continued until all twenty techniques within a particular data set were evaluated. The image that remained after this evaluation was identified as the best enhancement technique for that particular data set.

The third phase of the evaluation involved comparisons of the best enhanced image from each data set (i.e., Aircraft Multispectral Scanner, Landsat TM, etc.) to each other. This was accomplished using 11 individuals of varying expertise in remote sensing and photointerpretation. These individuals had no previous exposure to the data. The same criteria and methodology used for evaluating imagery within a data set were used for this comparison between data sets. This process continued until each person had individually selected the image that in his or her opinion was best for detecting off-road vehicular damage. Thus, the image that the majority of the photointerpreters selected was considered to represent the specific sensor and technique that would be best for detecting off-road vehicular damage. Additionally, the 11 interpreters individually ranked all nine images from best (1) to worst (9). Using this data, a Chi-square distribution was

calculated for the top three images selected by the interpreters to see if their selections were significantly better than chance selection.

3.4 CLASSIFICATION COMPARISON OF TWO SENSORS

The last specific sub-objectives for this research were to assess the impact of spatial resolution on classification performance of different cover types and to assess the interrelationships between sensor spatial resolution and forest and grassland cover types.

Geoscan's MKII Airborne Multispectral Scanner and Landsat TM were used in a comparison of classification accuracy performance. The LCTA plots that were located within the three study areas were divided into training plots and test plots. Plots having the same major vegetative cover types and approximately the same percent ground cover were identified, grouped together, and numbered. For each category of cover type and percent ground cover, odd numbered plots were used for test areas and even numbered plots were used for training areas. Appendix 1 lists LCTA plot information, identifying the training plots and test plots.

3.4.1 USE OF NORMALIZED DIFFERENCE VEGETATION INDEX

A Normalized Difference Vegetation Index (NDVI) was initially considered for inclusion in both data sets to aid in the classification of different vegetative cover types. However, other studies (Huete and Jackson 1987, Tueller 1987) have indicated that NDVI underestimates vegetation on light-

colored soil and overestimates vegetation on dark-colored soil.

To determine whether NDVI would aid in classifying vegetation at Pinon Canyon, Data Set 4 (Geoscan's MKII Airborne Multispectral Scanner) from Study Area 1 was first classified (unsupervised classification) using the three principal component bands and the NDVI band. A second data set was then created using only the three principal component bands. This new data set was classified in a similar manner and compared to the first classification. A test area was selected from an location that consisted of very light-colored background soil, with 10-20% vegetative cover uniformly distributed throughout the test area. This test area contained 172 pixels. The classification using the NDVI band classified 50 pixels as vegetation and 122 pixels as roads/exposed soil. The classification without NDVI, however, classified 101 pixels as vegetation and 71 pixels as roads/exposed soil. The estimate of vegetation present in the classification using the NDVI band was substantially lower than was actually present in this location. The classification without the NDVI band more accurately reflected the amount of vegetation present in this test area.

Another test area was selected from a location that consisted of very dark shale with little or no vegetation present. This test area contained 242 pixels. The classification using the NDVI classified 168 pixels as vegetation and 104 pixels as dark shale. The classification

without NDVI, however, classified 2 pixels as vegetation and 240 pixels as dark shale. The estimate of vegetation present in the classification using the NDVI band was substantially higher than was actually present in this location. The classification without the NDVI band more accurately reflected the amount of vegetation present in this test area.

A visual, qualitative evaluation of the two classifications was also done in these test areas. In locations that contained light-colored soil, the vegetation present as indicated by the classification using the NDVI band was much lower than was actually present. The vegetation present as indicated by the classification without the NDVI band, however, was much closer to the amount of vegetation actually present in that location.

Additionally, locations that contained the dark-colored shale with little or no vegetation were visually evaluated. The classification using the NDVI band indicated that there was an abundance of vegetation present in this location, where in fact, little or no vegetation was present.

These findings are consistent with the previous studies by Huete and Jackson (1987) and Tueller (1987). Therefore, to more accurately classify vegetation at Pinon Canyon, the NDVI channel was not used in the classification procedure.

3.4.2 CLASSIFICATION PROCEDURE

Because of the heterogeneity of this rangeland environment, an unsupervised classification technique was used

for classification. A mono-cluster blocks technique was used wherein small training blocks were extracted from each study area and mosaicked together (Fleming and Hoffer, 1977). These training blocks were carefully selected to ensure that each LCTA training plot was contained within at least one training block. Additionally, other training blocks were chosen to ensure that the maximum amount of spectral variability was contained in the mosaicked image. As much as possible, the same locations were chosen as training blocks in both data sets. Using the mosaicked images and an unsupervised statistical clustering algorithm within the ERDAS image processing system (ERDAS, Inc., 1990), a set of training signatures were developed for Data Set 8 and for each of the three study areas for Data Set 4.

After the training signatures were developed, each study area for both data sets was classified using the appropriate training data. Using ancillary information such as aerial photography, LCTA training plot information, and personal observation and on-site photographs taken by the author, the initial classes in the classified image were combined into like informational classes.

3.4.3 EVALUATION OF CLASSIFICATION ACCURACY

Classification accuracy for each data set was evaluated and compared using two methods. First, two sets of contingency tables of classification performance for the test areas in each data set were constructed. The first set of

contingency tables contained classification information about each informational class separately. The second set of contingency tables contained classification information about general cover types (i.e., forest, roads/exposed soil, and grasses). Overall classification accuracy was then calculated for each data set and for both types of contingency tables. The second approach used to compare classification accuracy was to determine if the classification accuracies of the two sensors were significantly different. To accomplish this, a set of polygons were digitized on each data set that corresponded to each test area (see Appendix 1). These test areas comprised half of the LCTA plots, as well as locations visited by the author in the field. These polygon files were then converted into geographic information system (GIS) files. Using the SUMMARY command within ERDAS, a cross-tabulation of pixels was developed to compare the polygon GIS files (i.e., "ground truth") and the classified GIS files.

An evaluation of overall classification accuracy of the two data sets was conducted by comparing the accuracies of the test areas on one data set to the accuracies of the same locations on the other data set. The percent of correctly classified pixels for each test area of the Landsat TM data was subtracted from the percent of correctly classified pixels for the same area in the Airborne Scanner data. Additionally, classification accuracies for the general cover types (forested areas, roads/exposed soil and rangeland grasses) were evaluated and compared. To accomplish this comparison,

the differences in classification accuracy were tested for normality.

The Kolmogorov-Smirnov goodness-of-fit test for normality (Zar 1984) was made for the differences in classification accuracy between the two data sets. Normality of the data was tested first for all categories, and then for the general cover types as described above. Upon completing this test, a null hypothesis that there was no difference between the two overall classification accuracies was tested using the Student's t-distribution. The above procedure was then followed to test for significant differences in classification accuracy between the general cover types (i.e., forest, roads/exposed soil and rangeland grasses). A similar hypothesis stated that there was no difference in classification accuracy between these general cover types.

3.4.4 INTERRELATIONSHIPS OF SENSOR SPATIAL RESOLUTION

To assess the interrelationships of sensor spatial resolution and forest and rangeland cover types, a portion of the Airborne Scanner and Landsat TM Data Sets were extracted from the original imagery. These sub-areas were converted into a format that was compatible with the MICROPIPS.EGA image processing system (MICROPIPS.EGA, The Telesys Group, Inc.) using a program called ERD2MP (Lee and Lee, 1990). A cross-sectional view of digital values for each pixel along a row of pixels, or scan line, was produced using MICROPIPS.EGA.

The result of this procedure was a set of figures that graphically depicted the variability in spectral response as a function of ground cover type and sensor spatial resolution. These figures summarized the differences in spectral variability that occurred between ground cover types, and helped explain differences in classification accuracy between sensors having different spatial resolution. The figures contain information from each portion of the electromagnetic spectrum (i.e., visible, near infrared and middle infrared). Scan line data from the Airborne Scanner and Landsat TM data (i.e., Data Sets 4 and 8) were combined onto the same page for visual comparison between sensor systems.

RESULTS AND DISCUSSION

4.1 DETECTION OF OFF-ROAD VEHICULAR DAMAGE

As previously mentioned in Chapter 3, a three-phase evaluation was conducted to determine which enhancement techniques and data sets most effectively enhanced tank trails. Phase one determined twenty enhancement technique/filter combinations that were applied to Study Area 1 (see Section 3.3.2).

During phase two of the evaluation, these twenty combinations were applied to nine data sets from a portion of Study Area 1. This resulted in 180 images in which tank trails were enhanced. Using three individuals and the evaluation criteria previously outlined, the enhanced images were compared within each data set. That is, for a particular data set, all twenty enhanced images were compared to determine the technique that best enhanced that particular type of remote sensor data. Based on these evaluations, the best technique for each data set is indicated by an asterisk on Table 4.1. Figures 4.1 through 4.9 are reproductions of the images selected as the best enhanced image for each data set.

In every case, the techniques that best enhanced tank trails utilized weighted Laplacian or 3 x 3 high-pass filters.

Table 4.1. Matrix used in evaluating enhancement techniques for different remote sensor systems. Asterisks within the cells denote the best enhancement technique for each particular data set.

	Laplacian (No Wt)	Laplacian (Filter 2)	Laplacian (Filter 3)	Sobel	Laplacian (5x5, No Wt)	Sobel w/Hi-Pass (3x3)	High-Pass (5x5)	Compass Gradients	Mero-Vassy	Prewitt	Chittineni	Vertical Gradient	Horizontal Gradient	Diag. Gradient (NW-SE)	Diag. Gradient (NE-SW)	Vert. and Horiz. Combined	Diagonal (Combined)	All Gradients combined	Isogradient	Raw Image
Enlarged Photo (Digitized) One Band		*																		
Digitized Photo One Band			*																	
Digitized Photo Three Bands		*																		
Aircraft MSS One Band		*																		
Aircraft MSS Three Bands		*																		
SPOT 10M Panchromatic				*																
SPOT/TM IHS Three Bands				*																
Landsat TM One Band				*																
Landsat TM Three Bands		*																		

Figure 4.1. Image selected as the best enhanced image from the enlarged NAPP photography (digitized). The Laplacian (Filter 2) filter was used for this enhancement.

Figure 4.2. Image selected as the best enhanced image from the digitized NAPP photography, one band. The Laplacian (Filter 3) filter was used for this enhancement.

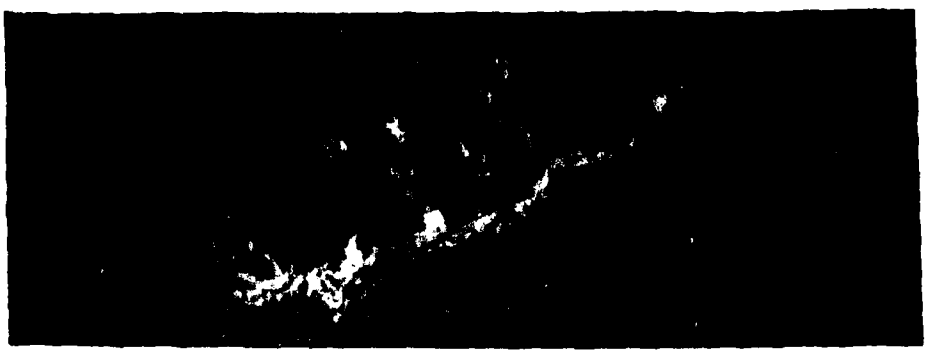

Figure 4.3. Image selected as the best enhanced image from the digitized NAPP photography, three bands. The Laplacian (Filter 2) filter was used for this enhancement.

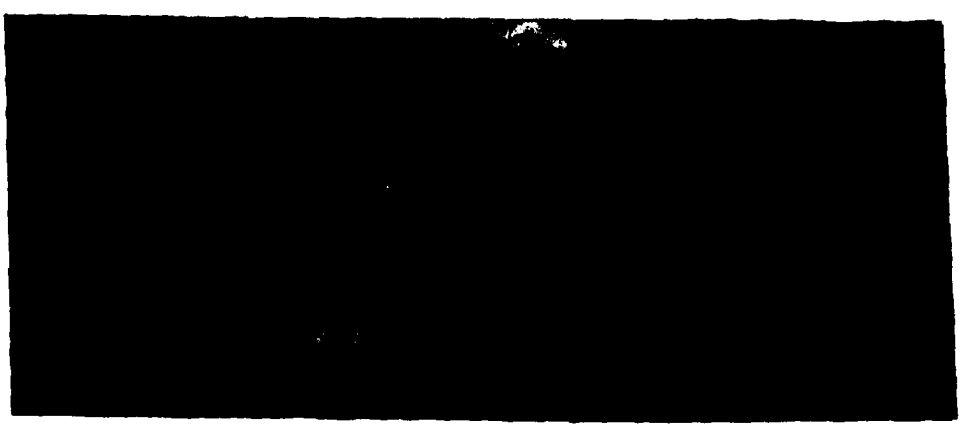

Figure 4.4. Image selected as the best enhanced image from the Airborne Multispectral Scanner, one band. The Laplacian (Filter 2) filter was used for this enhancement.

Figure 4.5 Image selected as the best enhanced image from the Airborne Multispectral Scanner, three bands. The Laplacian (Filter 2) filter was used for this enhancement.

Figure 4.6. Image selected as the best enhanced image from the SPOT Panchromatic data. The high-pass (3 x 3) filter was used for this enhancement.

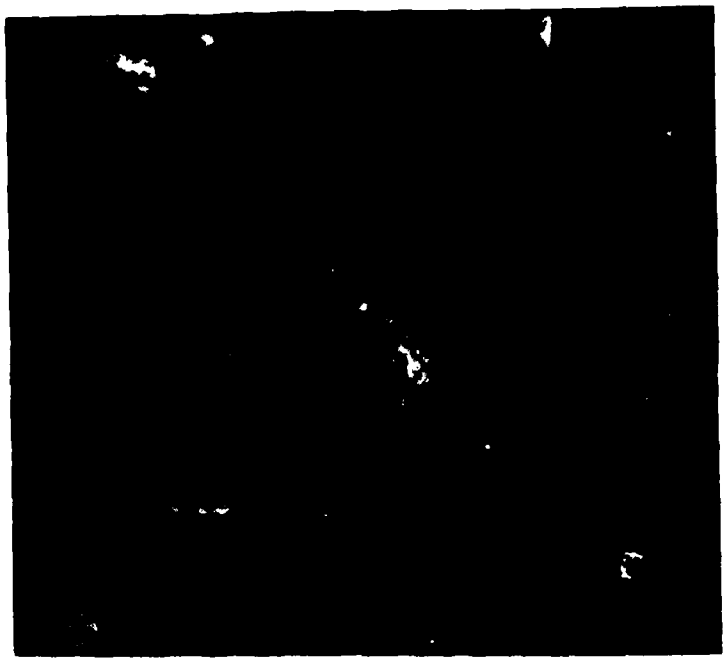

Figure 4.7. Image selected as the best enhanced image from the SPOT/TM intensity, hue, saturation transformation data. The high-pass (3 x 3) filter was used for this enhancement.

Figure 4.8. Image selected as the best enhanced image from Landsat Thematic Mapper, one band. The high-pass (3 x 3) filter was used for this enhancement.

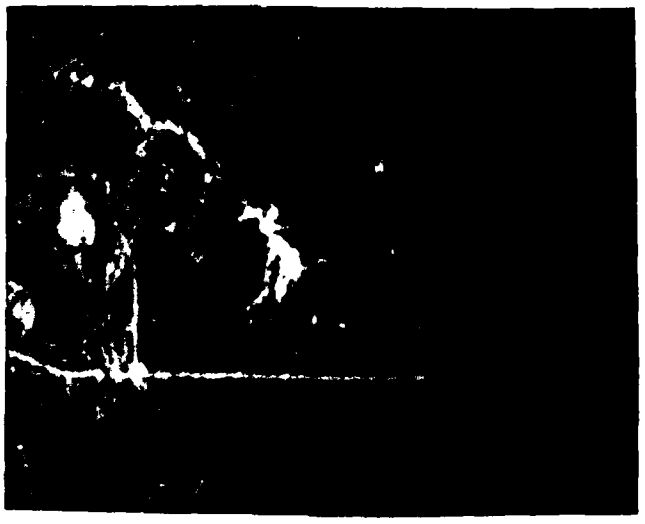

Figure 4.9. Image selected as the best enhanced image from Landsat Thematic Mapper, three bands. The Laplacian (Filter 2) filter was used for this enhancement.

Of the Laplacian filters, the filter that was selected as the most effective enhancement technique for most data sets was:

0	-1	0
-1	5	-1
0	-1	0

The other weighted Laplacian filter that best enhanced the one-band image of Data Set 5 was:

1	-2	1
-2	5	-2
1	-2	1

The filter that best enhanced tank trails in the other data sets was the 3 x 3 high-pass filter. This filter was:

-1	-1	-1
-1	9	-1
-1	-1	-1

The third phase of the evaluation compared the best enhanced image from each data set to like images in other data sets. Using the criteria previously outlined in Section 3.3.3, 11 individuals evaluated these images for their ability to enhance tank trails. Since there was a time delay between the acquisition dates of Data Set 1 (NAPP photography) and the rest of the imagery, interpreters were asked to compare just those tank trails that were visibly present in both images. The images were ranked from best (1) to worst (9). The results of this evaluation are summarized in Table 4.2.

Table 4.2. Matrix used in determining the best image and enhancement technique for detection of tank trails. Numbers in matrix refer to image rank as assigned by each individual.

Interpreter \ Data Set	Large Photo (Digitized) One Band	Digitized Photo One Band	Digitized Photo Three Bands	Aircraft MSS One Band	Aircraft MSS Three Bands	SPOT 10M Panchromatic	SPOT/TM IHS Three Bands	Landsat TM One Band	Landsat TM Three Bands
Person 1	4	5	6	3	1	2	7	9	8
Person 2	2	5	4	3	1	6	7	9	8
Person 3	3	6	5	2	1	4	7	9	8
Person 4	3	7	6	2	1	5	4	9	8
Person 5	4	7	6	2	1	3	5	9	8
Person 6	3	7	6	2	1	4	5	9	8
Person 7	4	7	6	2	1	3	5	9	8
Person 8	4	5	6	2	1	3	7	9	8
Person 9	2	6	5	3	1	4	7	9	8
Person 10	4	6	7	2	1	3	5	9	8
Person 11	4	6	7	2	1	3	5	9	8
Total Score	**37**	**67**	**64**	**25**	**11**	**40**	**64**	**99**	**88**

When the rank order of the images are summed down each column in Table 4.2, a total score for each data set is obtained. Low total scores represent data sets in which tank trails were easily detected. High total scores represent data sets in which tank trails were not easily detected. Of particular interest is the column of 1's down the middle of the table, and the lowest possible total score of 11. Every interpreter selected Geoscan's MKII Airborne Multispectral Scanner using three bands as the best image for enhancing tank trails. Several individuals selected the one-band image of the same sensor as the second best image for enhancing tank trails. It received a total score of 25.

It is interesting to note that the enlarged NAPP photography and the SPOT Panchromatic data sets received very similar scores of 37 and 40, respectively. This indicates that the ability of these two data sets to be enhanced for the detection of tank trails is approximately the same. Based on the number of pixels on the display screen that occurred along a known ground distance, the spatial resolution of the digitized enlarged NAPP photography was found to be approximately 5 meters. Surprisingly, the 10 meter spatial resolution SPOT Panchromatic data performed just as well as the 5 meter spatial resolution digitized enlarged NAPP photography. This is thought to be, in part, due to the "graininess" of the photography brought about by the photographic enlargement process. Another possibility may be the higher contrast present in the SPOT Panchromatic data

versus the digitized enlarged NAPP photography enabled easier identification of the tank trails.

The regular NAPP photography and the SPOT/TM intensity, hue, saturation transformation data sets also received similar scores. Again, this indicates that these data sets have similar capabilities in regard to enhancing tank trails.

On the bottom end of the scale, the Landsat TM Data Sets were very poor for detecting tank trails. They received scores of 88 and 99 for the three-band and one-band image, respectively. This is undoubtedly due to the larger 25 meter spatial resolution of this data.

When the original photography was video digitized, many fine details were lost. This was primarily a result of the type of equipment used for this process. The camera and video screen used were unable to capture many of the smaller tank trails that were clearly visible on the aerial photography. A flatbed or rotating drum scanner used for scanning positive transparencies of aerial photography would have undoubtedly produced an image of greater detail (Jensen 1986). This would have ensured that most of the fine tank trails would have been included in the digital imagery.

To evaluate the responses provided by the interpreters on the data sets used, a contingency table was created with each image listed across the top of the table and the possible ranking of these images down the left side (Table 4.3). The numbers in the matrix represent the number of interpreters that selected that particular ranking for each image.

Table 4.3. Performance ranking of images based on responses from interpreters.

		IMAGE[2]								
		1	2	3	4	5	6	7	8	9
RANK	1	0	0	0	0	11	0	0	0	0
	2	2	0	0	8	0	1	0	0	0
	3	3	0	0	3	0	5	0	0	0
	4	6	0	1	0	0	3	1	0	0
	5	0	3	1	0	0	1	5	0	0
	6	0	4	6	0	0	1	0	0	0
	7	0	4	2	0	0	0	5	0	0
	8	0	0	0	0	0	0	0	0	11
	9	0	0	0	0	0	0	0	11	0

It is obvious from Table 4.3 that an unusually high number of individuals ranked Images 5 and 4 as first and second best, respectively. Based on the information for image 5, a 95% confidence interval for the true percentage of individuals that would select this enhanced image as the best for detecting tank trails is (71.96 - 100). That is, 95 out of 100 times, 72% or more of the interpreters would select this image as the best enhanced image.

To further test the significance of interpreter responses, a Chi-square distribution was calculated for the interpreter's selection of the top three images to determine

[2]Images are as follows: 1) Large photo (digitized), one band, 2) Digitized photo, one band, 3) Digitized photo, three bands, 4) Aircraft AMSS, one band, 5) Aircraft AMSS, three bands, 6) SPOT 10M panchromatic, 7) SPOT/TM intensity, hue, saturation, three bands, 8) Landsat TM, one band, 9) Landsat TM, three bands.

whether the observed values were significantly different from those expected strictly by chance. Since there were only four images selected by the interpreters as the top three choices, two contingency tables were constructed with three rows and four columns each. Table 4.4 represents information from observed interpreter responses (extracted from Table 4.3). Table 4.5 represents expected frequencies of interpreter responses as determined strictly by chance. These were calculated from values in Table 4.4. Each expected cell value is equal to the row total multiplied by the column total, and divided by the grand total.

Table 4.4. Observed interpreter responses classified by image and ranking.

	IMAGE				
RANK	1	4	5	6	Row Total
1	0	0	11	0	11
2	2	8	0	1	11
3	3	3	0	5	11
Column Total	5	11	11	6	Grand Total=33

Table 4.5. Expected frequencies of interpreter responses if image and ranking were unrelated.

	IMAGE			
RANK	1	4	5	6
1	1.67	3.67	3.67	2.00
2	1.67	3.67	3.67	2.00
3	1.67	3.67	3.67	2.00

A Chi-square goodness-of-fit test measures significance between observed values and those expected strictly by chance. The test statistic for the Chi-square distribution is given by the following formula:

$$X^2 = \sum \frac{(observed\ cell\ count - expected\ cell\ count)^2}{(expected\ cell\ count)}$$

The null hypothesis (H_o) for this evaluation is that the differences reflected between the observed and expected frequencies in the interpreter's responses of image ranking are attributed to chance occurrence. The alternative hypothesis (H_a) is that the differences in the two values are not occurring strictly by chance. This would imply a direct relationship between an image and the ranking it received from the interpreters. The null hypothesis is rejected when the calculated value for Chi-square is greater than or equal to the critical value for Chi-square at the correct number of degrees of freedom. The number used for degrees of freedom (DF) is based on the size of the contingency table. It is determined according to the following equation:

DF = (Number of rows - 1)(Number of columns - 1)

Solving for DF in the equation above produces 6 degrees of freedom for use in the Chi-square calculations.

Following the form of the Chi-Square equation above, the Chi-square statistic becomes:

$$X^2 = \frac{(0 - 1.67)^2}{1.67} + \frac{(0 - 3.67)^2}{3.67} + \frac{(11 - 3.67)^2}{3.67} +$$

$$\frac{(0 - 2.00)^2}{2.00} + \frac{(2 - 1.67)^2}{1.67} + \frac{(8 - 3.67)^2}{3.67} + \frac{(0 - 3.67)^2}{3.67} +$$

$$\frac{(1 - 2.00)^2}{2.00} + \frac{(3 - 1.67)^2}{1.67} + \frac{(3 - 3.67)^2}{3.67} +$$

$$\frac{(0 - 3.67)^2}{3.67} + \frac{(5 - 2.00)^2}{2.00} = 37.38$$

This value exceeds the Chi-square critical value of 22.458 at $\alpha = .001$. Therefore, we reject the null hypothesis in favor of the alternative. That is, the differences between the observed and expected frequencies in the interpreter's responses of image ranking are not attributable to chance occurrence ($\alpha = .001$).

Since these differences are not attributable to chance, this indicates that there is indeed a relationship between a certain image and the number of interpreter's that selected it for a particular ranking. Thus, the selection of Images 5 and 4 (from Geoscan's MKII Airborne Multispectral Scanner) as the first and second best enhanced images, respectively, is not attributable to chance occurrence ($\alpha = .001$).

4.1.1 AERIAL PHOTOGRAPHY AND MULTISPECTRAL SCANNER COMPARISON

Since Image 5 (*Figure* 4.5) was selected as the best enhanced image by every interpreter in this research, a comparison was conducted between the actual aerial photography and Image 5 to determine the number of tank trails that were not being recorded, if any, by the multispectral scanner

(Image 5). The area covered by Image 5 was determined and identified on the NAPP aerial photography. The tank trails present in the aerial photography were carefully identified and marked to ensure that each trail was counted only once. This information was assumed to be a reference base from which comparison could be made with Image 5.

There were approximately three months after the aerial photography was acquired that U.S. Army units were allowed to train in this area. During this time, 2 new tank trails were made that are easily detected in Image 5. Therefore, less obvious tank trails could easily have been made, but the actual number is probably very small (5 to 10). Therefore, if all tank trails present in the aerial photography were visible in Image 5, and tank trails were made after the photography was obtained that are visible in Image 5, the total number of tank trails visible in Image 5 could conceivably exceed the number determined from aerial photography.

The number of tank trails visible in Image 5 was determined by placing a clear sheet of plastic over a computer display screen that had this image displayed. The visible trails were then carefully identified and marked to ensure each trail was counted only once. During these procedures, only the number of tank trails were considered, not the size of those trails.

There were 105 tank trails visible in Image 5. This includes all tank trails that may have been made during this three month time delay. The number of tank trails visible in

the aerial photography was 149. Therefore, considering that this estimate may be slightly high, 65-70% of the total number of tank trails visible in aerial photography were also visible in Image 5 (three band image created by Geoscan's MKII Airborne Multispectral Scanner).

From this information, it is obvious that although Geoscan's MKII Airborne Multispectral Scanner was selected as the best image for enhancing tank trails, a certain amount of detail was lost by capturing the information digitally rather than photographically. Most of this information, however, was the smaller trails that had been travelled on a very limited number of times (perhaps only once). Land managers must consider this loss of detail when using digital information to assess off-road vehicular damage.

A more quantitative approach in determining the actual amount of tank trail information recorded by a multispectral scanner could also be defined. Such an approach could be pursued as the subject of further research. First, the tank trails present in aerial photography could be digitized into a raster (grid cell) geographic information system. A binary map would be produced. A value of 1 would be assigned to every cell identified as tank trail, and a 0 would be assigned to everything else. The computer output would be a list of the total number of cells that included a tank trail, and those that did not.

The multispectral scanner imagery would be reclassified into a binary map. Again, a value of 1 would represent a tank

trail, and a value of 0 would represent everything else. The output would be the same as above. That is, a list of the total number of cells and their content would be provided. In this way, a direct comparison could be made between the two data sets of the total number of cells that contained tank trails.

4.1.2 RELATIVE COST COMPARISONS

A relative cost in terms of time required for the processing of the different enhancement techniques is provided for future users. First, any enhancement technique will take longer when applied to all bands in an image rather than just one of the bands. In the case of simple filtering operations such as directional line filters, high-pass, low-pass or the Laplacian filters, the time required increases proportionally with the number of bands subjected to the filtering process. These simple filtering operations are the most time efficient of all techniques attempted in this research, and appear to be the most effective.

Enhancement techniques that required a rotation of the filter by 90 degrees to create two images and the subsequent combining of these images in some manner was the next most time-consuming type of enhancement technique attempted. Examples of this type of technique were the Sobel, Mero-Vassy, and Prewitt operators. For the data used in this study, these rotational types of enhancement technique did not perform well.

The running difference or gradient type of enhancement techniques were the next most time-consuming technique. This technique required the creation of two images offset from each other by one pixel, and then subtracting one image from the other. This enhanced lines and edges in one direction only. The procedure was then repeated by creating two images offset from each other by one pixel in another direction and subtracting these two images. This procedure was satisfactory for lines in a particular orientation, but to obtain information about lines in other directions, these images needed to added together. Additionally, without a priori knowledge of where the tank trails were, it became difficult to identify tank trails as opposed to natural variations in topography and vegetation.

The isotropic gradient image suggested by Hord (1982) was the next most time-consuming enhancement technique. Rather than simply adding two gradient images together, the images were squared, added together, and the square root was taken. This produced slightly better results than simply adding the gradient images together, but required more time.

The most time-consuming enhancement technique of all those attempted was the combined directional line filter image. This technique combined the 8 images created with the directional line filters into one image using simple addition. This image enhanced major and secondary roads very well, but many of the fine tank trails were not discernable.

In summary, simple filtering operations such as the Laplacian filters were the most time efficient enhancement technique. The Laplacian filters also provided the best results of all techniques attempted in this research. Rotational filters (Sobel, Mero-Vassy, etc.) were the next most time-consuming technique and did not perform well for these data sets. Gradient and isotropic gradient images were the next most time-consuming techniques, respectively. They enhanced linear features rather well, but without a priori knowledge of where the tank trails were, it was difficult to distinguish between trails and natural variations in topography. The image that combined all directional line filters into one image was the next most costly technique. Major roads were enhanced, but small features were not discernable. Thus, the most effective was also, fortuitously, the most time efficient to utilize.

4.2 CLASSIFICATION COMPARISON OF TWO SENSORS

Portions of Pinon Canyon were classified using Geoscan's MKII Airborne Multispectral Scanner (referred to as Airborne Scanner in this section) with 6.5 meter spatial resolution and Landsat TM with 25 meter spatial resolution to compare classification accuracies between the two sensors.

Definitions for the informational classes in subsequent tables are as follows. Appendix 2 contains a partial list of vegetation found at Pinon Canyon and the abbreviations used in this research.

BOGR/HIJA 10-20% COVER	Blue grama (Bouteloua gracilis) and Galleta (Hilaria jamesii), approximately 10-20% ground cover.
BOGR/AGSM/HIJA 20-30% COVER	Blue grama (Bouteloua gracilis), Western wheatgrass (Agropyron smithii) and Galleta (Hilaria Jamesii), approximately 20-30% ground cover.
BOGR/SPAI/HIJA 30-40% COVER	Blue grama (Bouteloua gracilis), Alkali sacaton (Sporobolus airoides) and Galleta (Hilaria Jamesii), approximately 30-40% ground cover. Although occurring in many small clumps, Alkali sacaton tends to increase overall percent ground cover.
BOGR/SPAI/HIJA 40%+ COVER	Same as above. However, the small clumps of Alkali sacaton are larger, closer together and much more lush.
DARK SHALE 0-5% VEGETATIVE COVER	Predominantly occurring in small basins near shale outcrops. Very heavy concentration of shale with little or no vegetation.
SHALE-CLAY WITH AGSM/BOGR 20-30% COVER	Spectral response dominated by Shale-clay, similar to dark shale above. However, smaller amounts of shale mixed with clay allow mostly Western wheatgrass (Agropyron smithii) and Blue grama (Bouteloua gracilis) to be dominant species.

OPIM/BOGR/HIJA COVER	20-30%	Very distinctive plant community comprised of Tree cholla (Opuntia imbricata), Blue grama (Bouteloua gracilis) and Galleta (Hilaria jamesii). Tree cholla is the dominant overstory species.
JUMO/PIED/BOER CROWN CLOSURE	5-20%	Dominant species is One-seeded juniper (Juniperus monosperma) with occasional individuals of Pinyon pine (Pinus edulis). Open canopy areas are comprised of Black grama (Bouteloua eriopoda) with lesser amounts of Blue grama (Bouteloua gracilis) and Galleta (Hilaria jamesii).
JUMO/PIED/BOER CROWN CLOSURE	20-30%	Same as above. However, the overstory of One-seeded juniper and occasional Pinyon pine has a crown closure of approximately 20-30%.
JUMO/PIED/BOER CROWN CLOSURE	30-50%	Same as above. However the crown closure is approximately 30-50%.
ROADS/EXPOSED SOIL 0-10% VEGETATIVE COVER		Predominantly roads, but also includes areas of very sparse vegetation on limestone ridges or prairie dog towns.
SEMI-RIPARIAN VEGETATION (TAPE)		Vegetation predominantly in study area 3 below check dams in the arroyos. The slow trickle of groundwater from the arroyo ponds allows vegetation such as Five-stamen tamarix (Tamarix pentandra) and other grasses to survive.

ANNUALS BY DISTURBED AREAS	Annual vegetation caused by ground disturbance of tanks and other vehicles. Predominant species is the Russian thistle (Salsola iberica).

The three study areas from the Airborne Scanner and Landsat TM were classified using an unsupervised maximum likelihood classification algorithm. Tables 4.6 through 4.9 indicate the spectral classes for each data set and study area and the informational classes into which they were classified.

Table 4.6. Spectral and informational classes for the Airborne Scanner, Study Area 1.

CLASS NUMBER	SPECTRAL CLASSES	INFORMATIONAL CLASS*
1	7, 14, 15, 23, 24	BOGR/HIJA 10-20% COVER
2	13	OPIM/BOGR/HIJA 20-30% CVR
3	1, 2, 3, 4, 6, 9, 16, 18, 28	BOGR/AGSM/HIJA 20-30% CVR
4	8, 17, 19, 20	BOGR/SPAI/HIJA 30-40% CVR
5	25	BOGR/SPAI/HIJA 40%+ COVER
6	21, 22	DARK SHALE 0-5% VEGETATION
7	26, 27	SHALE-CLAY AGSM/BOGR 20-30% COVER
8	5, 10, 11, 12	ROADS/EXPOSED SOIL 0-10% COVER
9	29	BACKGROUND

* A partial list of vegetation cover types found at Pinon Canyon and abbreviations used is found in Appendix 2.

Table 4.7. Spectral and informational classes for the Airborne Scanner, Study Area 2.

CLASS NUMBER	SPECTRAL CLASSES	INFORMATIONAL CLASS
1	1, 2, 7, 9, 13	BOGR/HIJA 10-20% COVER
2	4, 6, 14, 19	BOGR/AGSM/HIJA 20-30% CVR
3	5, 20, 22	BOGR/SPAI/HIJA 30-40% CVR
4	8, 21	ANNUALS BY DISTURBED AREAS
5	12	BOGR/SPAI/HIJA 40%+ COVER
6	15	ROADS/EXPOSED SOIL 0-10% COVER
7	3, 10, 11, 16, 17, 18	OPIM/BOGR/HIJA/JUMO 20-30% COVER

Table 4.8. Spectral and informational classes for the Airborne Scanner, Study Area 3.

CLASS NUMBER	SPECTRAL CLASSES	INFORMATIONAL CLASS
1	1, 2, 3, 6, 7, 8, 10, 11, 15, 18, 21, 22, 30	BOGR/HIJA 10-20% COVER
2	4, 9, 14, 16, 19, 20, 24, 25, 27, 28, 29, 34	BOGR/AGSM/HIJA 20-30% CVR
3	5, 12	SEMI-RIPARIAN VEG. (TAPE)
4	13, 17	ROADS/EXPOSED SOIL 0-10% COVER
5	26	BOGR/SPAI/HIJA 30-40% CVR
6	33	JUMO/PIED/BOER 5-20% CROWN CLOSURE
7	31	JUMO/PIED/BOER 20-30% CROWN CLOSURE
8	23, 32, 35	JUMO/PIED/BOER 30-50% CROWN CLOSURE
9	36	BACKGROUND

Table 4.9. Spectral and informational classes for Landsat TM, Study Areas 1-3.

CLASS NUMBER	SPECTRAL CLASSES	INFORMATIONAL CLASS
1	1, 8, 12, 19	BOGR/HIJA 10-20% COVER
2	6, 7, 9, 11, 15, 20, 21, 30	BOGR/AGSM/HIJA 20-30% COVER
3	10, 14, 16, 28	BOGR/SPAI/HIJA 30-40% COVER
4	17, 23, 26	BOGR/SPAI/HIJA 40%+ COVER
5	22	DARK SHALE 0-5% VEG COVER
6	24	SHALE-CLAY AGSM/BOGR 20-30% COVER
7	5, 13, 18	OPIM/BOGR/HIJA 20-30% COVER
8	4	JUMO/PIED/BOER 5-20% CROWN CLOSURE
9	27, 29	JUMO/PIED/BOER 20-30% CROWN CLOSURE
10	3, 31	JUMO/PIED/BOER 30-50% CROWN CLOSURE
11	25	ROADS/EXPOSED SOIL 0-10% COVER
12	32	BACKGROUND

4.2.1 CLASSIFICATION COMPARISON

Overall classification accuracy for a contingency table is determined by summing the number of correctly classified pixels for each category (the major diagonal from top left to lower right) and dividing this number by the total number of pixels or samples used (Story and Congalton, 1986). For an overall classification comparison, test area information from the three study areas from the Airborne Scanner were combined into one contingency table (Table 4.10). Table 4.11 is a contingency table depicting classification performance of the Landsat TM data. The numbers in the cells of these two tables represent the number of pixels that were classified into a

Table 10. Contingency table for classification of the Airborne Scanner data (all three study areas combined).

	BOGR/HIJA 10-20% CVR	BOGR/AGSM/HIJA 20-30% COVER	BOGR/SPAI/HIJA 30-40% COVER	BOGR/SPAI/HIJA 40%+ COVER	DARK SHALE 0-5% VEGETATIVE COVER	SHALEY-CLAY AGSM/BOGR 20-30% COVER	OPIM/BOGR/HIJA 20-30% COVER	JUMO/PIED/BOER 5-20% CROWN CLOSURE	JUMO/PIED/BOER 20-30% CROWN CLOSURE	JUMO/PIED/BOER 30-50% CROWN CLOSURE	ROADS/EXPOSED SOIL 0-10% COVER	ANNUALS ALONG DISTURBED AREAS	SEMI-RIPARIAN VEGETATION (TAPE)	ROW TOTALS
BOGR/HIJA 10-20% COVER	1159	103	7	14		23	46				33	28	2	1415
BOGR/AGSM/HIJA 20-30% COVER	56	890	61	14			61				6	37		1125
BOGR/SPAI/HIJA 30-40% COVER	5	47	192	15		1	28							288
BOGR/SPAI/HIJA 40%+ COVER		32		196						27				255
DARK SHALE 0-5% VEGETATIVE COVER		5			730	14								749
SHALE-CLAY AGSM/BOGR 20-30% COVER	83	13	19	15	7	371								508
OPIM/BOGR/HIJA 20-30% COVER		15	1				157							173
JUMO/PIED/BOER 5-20% CROWN CLOSURE	33	59	7					91		1	2		1	194
JUMO/PIED/BOER 20-30% CROWN CLOSURE	93	268	15	18					228	28		30		680
JUMO/PIED/BOER 30-50% CROWN CLOSURE	3	47	3	24					1	560				638
ROADS/EXPOSED SOIL 0-10% COVER	11	3	1	1					3		212	19		250
ANNUALS ALONG DISTURBED AREAS	49	5					1				15	247		317
SEMI-RIPARIAN VEGETATION (TAPE)	121	40									10		120	291
COLUMN TOTALS	1613	1527	306	297	737	409	293	91	232	616	278	361	123	**6883**

Table 4.11. Contingency table for classification of the Landsat Thematic Mapper Data.

	BOGR/HIJA 10-20% CVR	BOGR/AGSM/HIJA 20-30% COVER	BOGR/SPAI/HIJA 30-40% COVER	BOGR/SPAI/HIJA 40%+ COVER	DARK SHALE 0-5% VEGETATIVE COVER	SHALEY-CLAY AGSM/BOGR 20-30% COVER	OPIM/BOGR/HIJA 20-30% COVER	JUMO/PIED/BOER 5-20% CROWN CLOSURE	JUMO/PIED/BOER 20-30% CROWN CLOSURE	JUMO/PIED/BOER 30-50% CROWN CLOSURE	ROADS/EXPOSED SOIL 0-10% COVER	ROW TOTALS
BOGR/HIJA 10-20% COVER	565	105	16	2		1	24	2	16		6	737
BOGR/AGSM/HIJA 20-30% COVER	126	754	2	8			4		1			895
BOGR/SPAI/HIJA 30-40% COVER	18	7	107	28		4	20					184
BOGR/SPAI/HIJA 40%+ COVER	6	4	48	138			3					199
DARK SHALE 0-5% VEGETATIVE COVER		3			36	1						40
SHALE-CLAY AGSM/BOGR 20-30% COVER		18		4		146	3					171
OPIM/BOGR/HIJA 20-30% COVER	4			3		2	93					102
JUMO/PIED/BOER 5-20% CROWN CLOSURE	6	10		1			1	83	1	1		103
JUMO/PIED/BOER 20-30% CROWN CLOSURE	16	12			1	1	2	3	167	7		209
JUMO/PIED/BOER 30-50% CROWN CLOSURE	1						2		1	475		479
ROADS/EXPOSED SOIL 0-10% COVER	174	10				1	4		63		380	632
COLUMN TOTALS	916	923	173	184	37	156	156	88	249	483	386	**3751**

certain category. Only those informational classes that were coincident in both data sets were used in the classification comparison (due to differences in spatial resolution and the very limited extent of their occurrence, two informational classes were not identified using Landsat TM, namely the annual vegetation along disturbed areas, and the semi-riparian vegetation found downslope from the arroyo dams).

Overall classification accuracy for the Airborne Scanner and Landsat TM (individual cover types) was calculated from Tables 4.10 and 4.11 as follows:

Airborne Scanner (from Table 4.10):

Sum of the major diagonal = 5153
Total number of pixels (samples) = 6883
Overall classification accuracy = 5153/6883 = 74.9%

Landsat TM (from Table 4.11):

Sum of the major diagonal = 2944
Total number of pixels (samples) = 3751
Overall classification accuracy = 2944/3751 = 78.5%

In addition, contingency tables were created that combined the information shown in Tables 4.10 and 4.11 into general cover type groups for the Airborne Scanner and Landsat TM (Tables 4.12 and 4.13, respectively). These included forested areas, roads/exposed soil, grassland classes and other (other classes include dark shale, annuals along disturbed areas and semi-riparian vegetation).

Overall classification accuracies for the Airborne Scanner and Landsat TM (combining general cover types) were calculated from Tables 4.12 and 4.13 as follows:

Table 4.12. Contingency table for combined general cover types for classification of the Airborne Scanner (all study areas combined).

	Forested Areas	Roads/Exp. Soil	Grassland Areas	Others	Row Totals
Forested Areas	909	2	570	31	1512
Roads/Exp Soil	3	212	16	19	250
Grassland Areas	27	39	3631	67	3764
Others	0	25	235	1097	1357
Column Totals	939	278	4452	1214	**6883**

Table 4.13. Contingency table for combined general cover types for classification of Landsat TM.

	Forested Areas	Roads/Exp. Soil	Grassland Areas	Others	Row Totals
Forested Areas	738	0	52	1	791
Roads/Exp Soil	63	380	189	0	632
Grassland Areas	19	6	2263	0	2288
Others	0	0	4	36	40
Column Totals	820	386	2508	37	**3751**

Airborne Scanner (from Table 4.12):

Sum of the major diagonal = 5849
Total number of pixels (samples) = 6883
Overall classification accuracy = 5849/6883 = 85.0%

Landsat TM (from Table 4.13):

Sum of the major diagonal = 3417
Total number of pixels (samples) = 3751
Overall classification accuracy = 3417/3751 = 91.1%

When general cover types were combined in Tables 4.12 and 4.13, overall classification accuracy was improved approximately 10% and 12% for the Airborne Scanner and Landsat TM, respectively. This indicates that much of the error that was occurring in Tables 4.10 and 4.11 was due to misclassification between similar cover types (i.e., 20-30% grass cover was classified as 10-20% grass cover, etc.).

The results of overall classification, as calculated from data in Tables 4.10 through 4.13, are good classification results. Classification accuracies of 75 to 80% for individual classes such as those identified in this research is good. Additionally, according to Anderson et al. (U.S. Department of the Interior, 1976), the information contained within the general cover type groups used in this research are considered to be Level I land use and land cover categories. The minimum level of acceptable classification accuracy for Level I land use and land cover categories using satellite remote sensor data should be at least 85% (U.S. Department of the Interior, 1976). According to the the above information for the general cover type groups, this goal has been met.

It is also important to note that in both cases, Landsat TM produced a higher overall classification accuracy than Geoscan's MKII Airborne Multispectral Scanner. This is, in part, due to the spatial resolution differences between the sensors. A detailed discussion concerning differences in classification accuracy as a function of sensor spatial resolution and cover type, along with any significant differences in classification accuracy is deferred until later.

To determine whether there were significant differences in classification accuracy between the two data sets, polygons were digitized on each data set that corresponded to the different test areas. The percent of correctly classified pixels in Landsat TM was subtracted from the percent of correctly classified pixels for the same area in the Airborne Scanner. Thus, a resulting value of 0 represents a test area that was classified with the same percent accuracy for both sensors. Similarly, a positive value represents a test area in which the Airborne Scanner produced a higher percent of correctly classified pixels than did Landsat TM. A negative value represents a test area where Landsat TM had a higher percent of correctly classified pixels than did the Airborne Scanner. The results of this comparison are summarized in Table 4.14.

Table 4.14. Differences in percent of correctly classified pixels for test areas in the Airborne Scanner and Landsat TM.

FORESTED AREAS	ROADS/EXPOSED SOIL		GRASSLAND AREAS	
-50.83	28.79	33.03	- 7.73	-11.18
-57.83	11.46	22.41	11.23	-12.35
-24.72	30.93	24.14	- 3.98	9.70
-22.44	19.05	35.10	6.85	- 5.72
-25.54	10.75		7.46	6.67
-27.93	19.45		-13.51	10.91
- 8.28	41.77		1.46	0.21
			2.82	3.96
			- 0.43	
MEAN = -31.08	MEAN = 25.17		MEAN = 0.37	
STD DEV = 17.23	STD DEV = 9.78		STD DEV = 8.21	

OVERALL STATISTICS:
MEAN = 1.88
STANDARD DEVIATION = 22.64

The student's t-distribution was used to test for significant differences between the classification accuracies of the Airborne Scanner and Landsat TM. One of the assumptions that must be met before using the student's t-distribution is that the data be normally distributed. To test the data in Table 4.14 for normality, the Kolmogorov-Smirnov goodness-of-fit test for normality was used. The tabular data required to perform this test and the subsequent calculations are in Appendix 4. The result was that the data in Table 4.14 were normally distributed, both collectively and for the individual general cover types.

4.2.2 TESTS FOR DIFFERENCES IN CLASSIFICATION ACCURACY

Since the above data are normally distributed, a student's t-distribution was used to test for significant

differences between classification accuracies. For these tests, the following test procedures were used:

Step 1: H_o: $\mu = 0$ (That is, the null hypothesis was that the true mean of the differences between classification accuracies of the two sensors was zero, implying no significant difference in classification accuracy between the two sensors for the cover types involved).

Step 2: H_a: $\mu \neq 0$ (That is, the true mean of the differences between classification accuracies of the two sensors was not zero, implying that there was a significant difference between the two sensors for the cover types involved).

Step 3: $\alpha = .01$ (That is, the data were tested at the $\alpha = .01$ level of significance).

Step 4: Test statistic used: $$t = \frac{(\bar{x} - 0)}{s / \sqrt{n}}$$

Where $\bar{x}$ = sample mean

s = sample standard deviation

and n = number of observations

Step 5: The rejection region was identified.

(That is, H_o was rejected if $|t| \geq t_{\alpha,n-1}$ where $t_{\alpha,n-1}$ is the critical value for t at α=.01 and n-1 degrees of freedom).

Step 6: The value of t was calculated according to the equation in step 4.

Step 7: A decision was made based on the parameters outlined above.

The following sections summarize the student's t-tests that were conducted for an overall classification accuracy assessment, as well as for general cover types individually.

ALL GENERAL COVER TYPES COMBINED:

$t_{calculated}$ (from step 4) = 0.49

$t_{critical}$ (from statistical table) = 2.73

Since $t_{calculated} \not\geq t_{critical}$, H_o was not rejected. That is, at $\alpha = .01$, there is no significant difference in classification accuracies between the two sensors when all general cover types are combined.

FORESTED AREAS:

$t_{calculated}$ (from step 4) = 4.77

$t_{critical}$ (from statistical table) = 3.71

Since $t_{calculated} \geq t_{critical}$, H_o was rejected. That is, at $\alpha = .01$, there is a significant difference in classification accuracies between the two sensors when forested areas only are considered.

ROADS/EXPOSED SOIL:

$t_{calculated}$ (from step 4) = 8.55

$t_{critical}$ (from statistical table) = 3.17

Since $t_{calculated} \geq t_{critical}$, H_o was rejected. That is, at $\alpha = .01$, there is a significant difference in classification accuracies between the two sensors when roads/exposed soil only are considered.

GRASSLAND AREAS:

$t_{calculated}$ (from step 4) = 0.19

$t_{critical}$ (from statistical table) = 2.92

Since $t_{calculated} \geq t_{critical}$, H_0 was not rejected. That is, at $\alpha = .01$, there is no significant difference in classification accuracies between the two sensors when grassland cover types only are considered.

As these results indicate, there is no significant difference in classification accuracies between the Airborne Scanner and Landsat TM when all general cover types are considered. However, when the individual general cover type differences are examined, significant differences are noted. For instance, there is a significant difference ($\alpha = .01$) between classification accuracies for the forest cover types. Table 4.14 indicates that in every case, the differences in classification accuracy were negative. As previously noted, this indicates that Landsat TM had better classification accuracy performance than the Airborne Scanner for forest cover types. This is consistent with earlier work (Kan et al., 1975; Sadowski et al., 1977; Latty and Hoffer, 1981; Badhwar et al., 1984; Haack et al., 1987) wherein it was found that sensors with a lower (coarser) spatial resolution often obtained higher classification accuracies than did sensors with higher (finer) spatial resolution. This is due to the higher pixel to pixel variation present in the imagery obtained from higher spatial resolution sensors. The lower spatial resolution sensors have less variation from pixel to pixel, and thus produce higher classification accuracies.

Additionally, there is a significant difference ($\alpha = .01$) between classification accuracies for cover types such as

road/exposed soil. Table 4.14 indicates that the differences in classification accuracy were positive in every case. This indicates that the Airborne Scanner had better classification accuracy performance than Landsat TM for cover types such as road/exposed soil that are small and have a high percentage of boundary pixels per unit area. As previous studies have indicated (Morgenstern et al., 1977; Landgrebe et al., 1977; Markham and Townshend, 1981), this is an advantage of the higher spatial resolution sensors. A higher percentage of the pixels in a higher spatial resolution sensor are included within the boundaries of an informational class. This reduces the number of edge and boundary pixels, and thus increases classification accuracy within these cover types.

There was no significant difference in classification accuracy between the two sensors for the grassland cover types. This makes sense because the variability in a natural grassland cover type is relatively low and constant. That is, the spectral variation over a small portion of grassland (6.5 x 6.5 meters) will be approximately the same as the variation over a much larger area of grassland (25 x 25 meters) containing the same cover types. These findings are also consistent with earlier work (Latty and Hoffer, 1981). Classification accuracies of high spatial resolution sensors and low spatial resolution sensors will be similar for cover types of low spectral variability (i.e., agricultural fields, pasture and grasslands, etc.).

Since there was such dramatic differences in classification accuracy between major cover type groups, it seems counter-intuitive that there was no significant difference in classification accuracy when all cover types were combined. One possible explanation is that the significant differences exhibited between the sensors in the individual cover types were of similar magnitude in opposing directions so as to offset each other. In other words, the impact of high classification accuracy in the Airborne Scanner within the road/exposed soil cover types was offset by the low classification accuracy in Landsat TM within the same cover types. Similarly, the impact of poor classification accuracy of the Airborne Scanner in the forested cover types was offset by the high classification accuracy in Landsat TM within these forested areas.

The proportion of pixels taken as test data for the different cover types was approximately proportional to the actual cover types found at Pinon Canyon over the study areas. Thus, the relationships of classification accuracy as described above would be applicable to the entire study area.

4.3 INTERRELATIONSHIPS OF SENSOR SPATIAL RESOLUTION

A comparison between portions of Geoscan's MKII Airborne Multispectral Scanner (Data Set 4) and Landsat TM (Data Set 8) was conducted to document the interrelationships of spatial resolution between forest and rangeland cover types. As mentioned in Chapter 3, a cross-sectional view of digital

values across one scan line was obtained using MICROPIPS.EGA. Figures 4.10 through 4.12 are graphical representations of these cross sections. Figure 4.13 is a reproduction of the area from which the scan lines were taken. Figure 4.13 is a portion of Study Area 3 from the Airborne Scanner data.

These graphs were taken from a scan line that crossed forest cover types such as One-seeded juniper (Juniperus monosperma) and Pinyon pine (Pinus edulis). These cover types are located on the left portion of the graphs as indicated.

The scan line also covered rangeland grasses such as Blue grama (Bouteloua gracilis), Galleta (Hilaria jamesii), Alkali sacaton (Sporobolus airoides) and Western wheatgrass (Agropyron smithii). These cover types are located on the right portion of the graphs.

Statistics were obtained for the forested area as well as the grassland area for the scan lines. These statistics help in understanding Figures 4.10 through 4.12. Table 4.15 summarize these statistics.

Table 4.15. Mean and standard deviation of forest and grassland cover types for the Airborne Scanner and Landsat TM. Top number is the mean with standard deviation in parentheses.

	Airborne Scanner			Landsat TM		
	Visible	Near-IR	Mid-IR	Visible	Near-IR	Mid-IR
Forested Area	94.19 (43.79)	102.45 (39.73)	103.10 (46.16)	106.13 (26.06)	84.97 (6.55)	95.08 (26.82)
Grassland Area	111.98 (15.09)	105.27 (16.48)	115.15 (14.30)	115.24 (13.97)	74.38 (4.67)	135.04 (16.50)

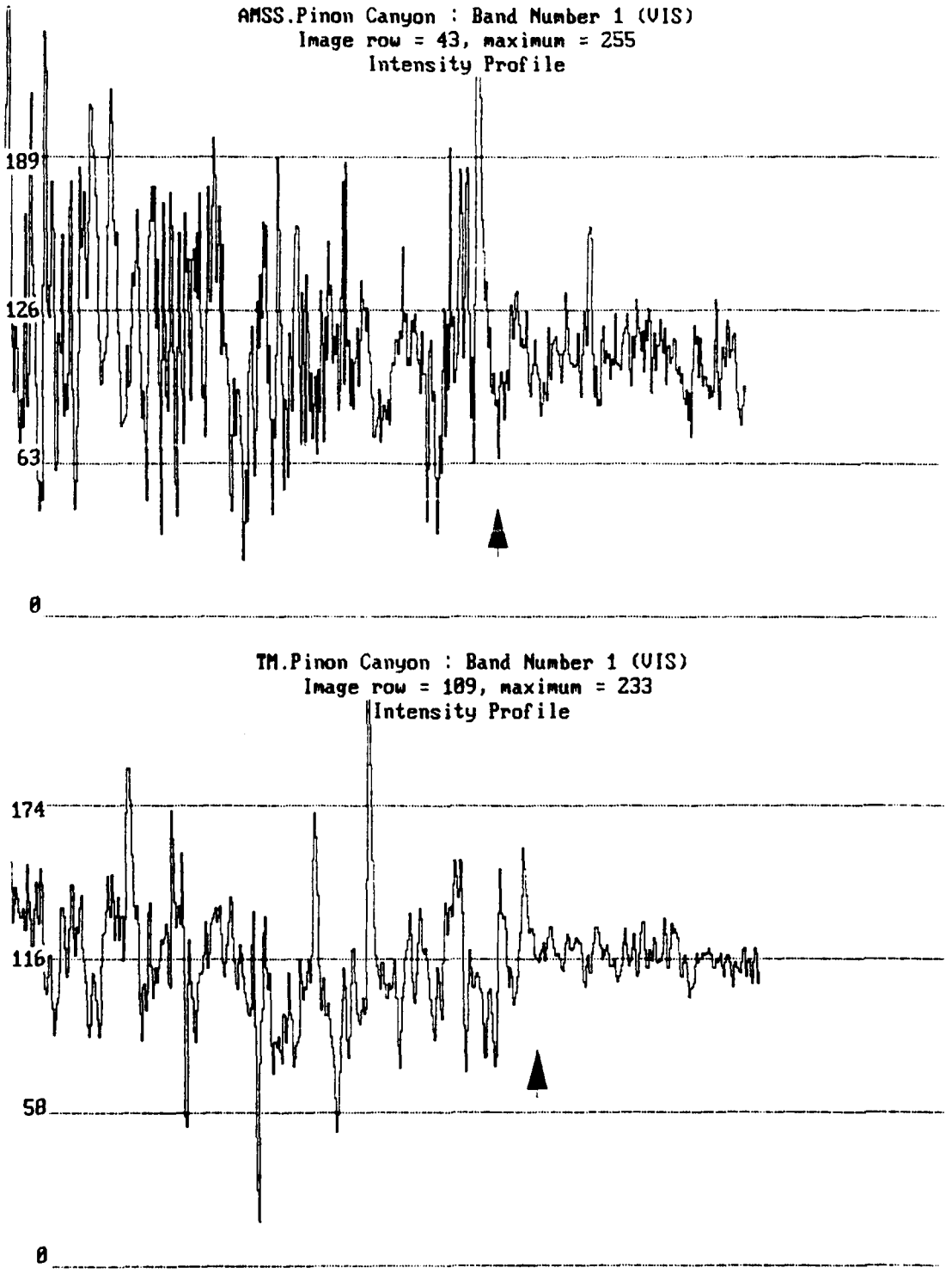

Figure 4.10. Profile of a scan line from the visible portion of the Airborne Scanner data (Data Set 4), top, and the Landsat TM data (Data Set 8), bottom. Scan line was taken across forest cover types (left) and grassland cover types (right). The change from forest to grass is identified by the arrowhead.

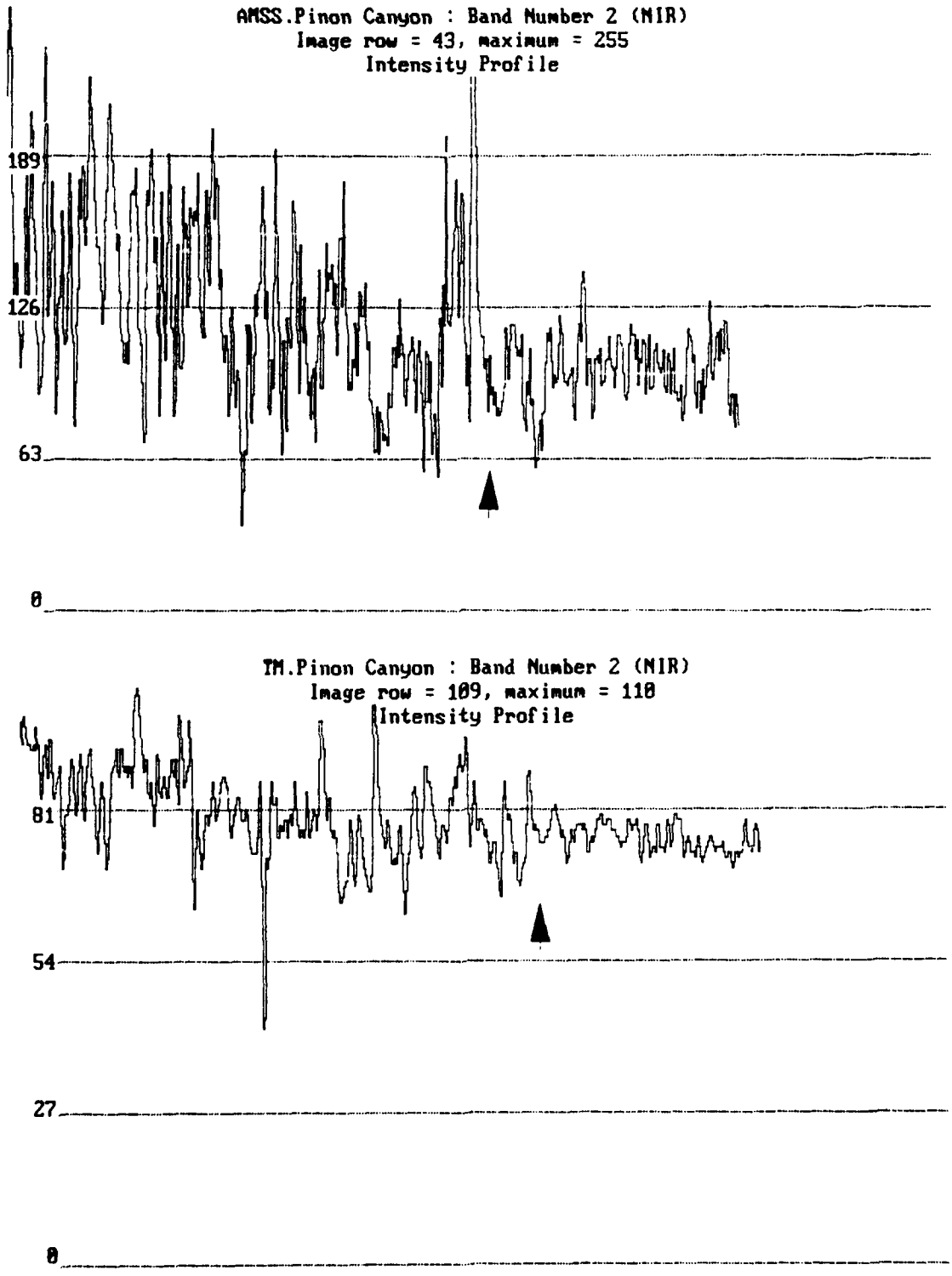

Figure 4.11. Profile of a scan line from the near-infrared portion of the Airborne Scanner data (Data Set 4), top, and the Landsat TM data (Data Set 8), bottom. Scan line was taken across forest cover types (left) and grassland cover types (right). The change from forest to grass is identified by the arrowhead.

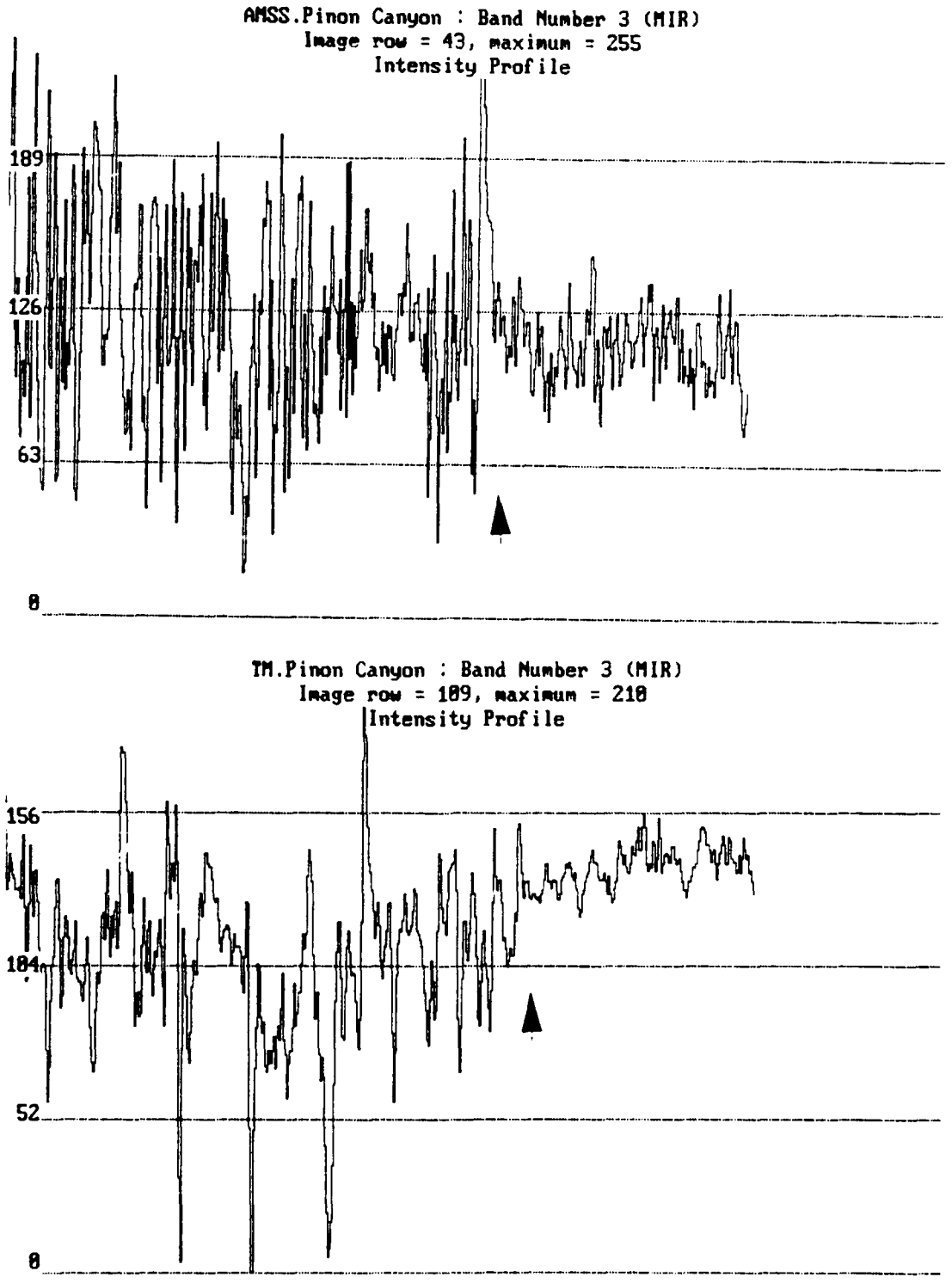

Figure 4.12. Profile of a scan line from the middle-infrared portion of the Airborne Scanner data (Data Set 4), top, and the Landsat TM data (Data Set 8), bottom. Scan line was taken across forest cover types (left) and grassland cover types (right). The change from forest to grass is identified by the arrowhead.

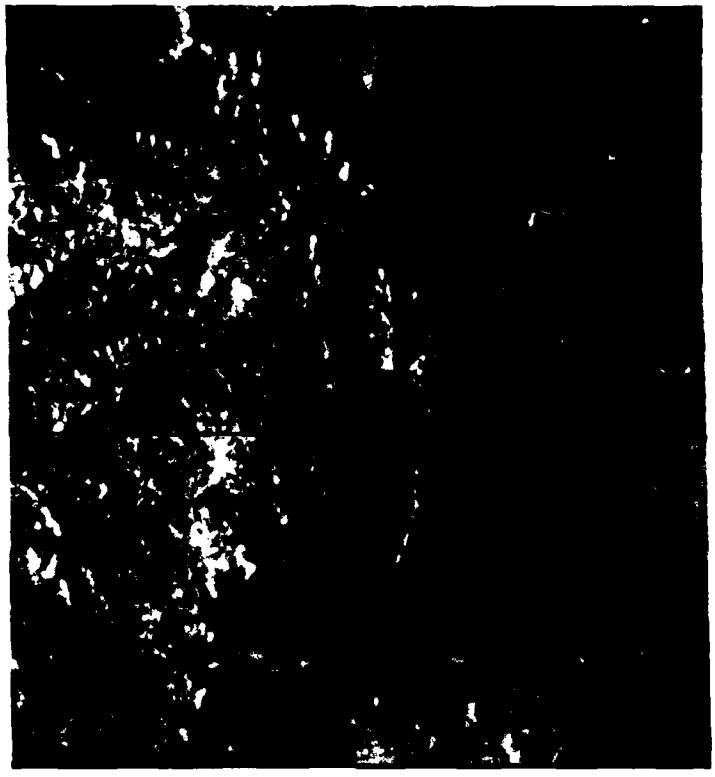

Figure 4.13. Photographic reproduction of a portion of Study Area 3 from Geoscan's MKII Airborne Multispectral Scanner. The black line marks the location of the scan line profiles taken from this area.

As reflected by Table 4.15, the standard deviation, and thus the variance, of data values within forested areas for the Airborne Scanner are higher than those for Landsat TM. This is true for every band. In addition, the standard deviation of data values within grassland areas for the Airborne Scanner are approximately similar to those for Landsat TM. The only exception is the near-infrared band.

This is primarily due to the highly variable canopy within the forest cover types. There are many open spaces between the tree crowns at Pinon Canyon. These open spaces are usually covered to some degree by grasses, but in some areas may be completely void of vegetation. Grassland cover types, on the other hand, are basically homogeneous throughout the entire grassland community, thus producing a lower variation of data values.

The high spatial resolution of the Airborne Scanner (6.5 meters) allows individual pixels to detect information between tree crowns such as grass or bare ground. Other pixels may record information from the shady side of a large tree, whereas its immediate neighbor may record information from the sunny side of the same tree crown. This concept of high variability from pixel to pixel is graphically displayed on the left portion (forested areas) of Figures 4.10 (top) through 4.12 (top).

The lower spatial resolution of Landsat TM (25 meters), on the other hand, allows many of these irregularities in the tree canopy to be averaged into the information recorded by

one larger pixel. Thus the potential for high variability from pixel to pixel is reduced by sensors with lower spatial resolution. This concept of averaging the variability within the tree canopy and thus reducing the variability from pixel to pixel is displayed in the left portion (forested areas) of Figures 4.10 (bottom) through 4.12 (bottom).

The right portion of Figures 4.10 through 4.12 is a graphic representation of data values taken over a grassland community. As is visually interpreted, the variance is drastically reduced as compared to forest communities for both sensor systems.

Relating these findings back to the classification comparison between the two sensor systems, many interesting facts are noted. First, there was a significant difference (α = .01) in classification accuracy between the two sensor systems for forest cover types. Specifically, Landsat TM provided the better classification in these cover types. The reduction in spectral variance from pixel to pixel in Landsat TM (which has the lower, or coarser, spatial resolution), was the reason forest cover types were classified higher with this system.

Second, there was a significant difference (α = .01) in classification accuracy between the two sensors for road/exposed soil cover types. In this case, the Airborne Scanner produced the better classification. The higher (finer) spatial resolution of the Airborne Scanner enabled more pixels to be included in the actual cover type and a

lower proportion of pixels to be included in boundary between cover types. This increased classification accuracy for these cover types for the Airborne Sensor.

Third, there was no significant difference ($\alpha = .01$) in classification accuracies between the two sensors for grassland cover types. This is due to the fact that the spectral variation from pixel to pixel in these cover types was reduced due to the nature of the cover type involved. Grassland communities have similar variation over a small area as compared to a larger area.

As previously mentioned, the differences in classification accuracy between the two sensors when all general cover types were involved was not significantly different. This is due to the fact that differences in individual cover types were in opposing directions so as to offset each other.

SUMMARY AND CONCLUSIONS

5.1 SIGNIFICANT RESULTS

This research has produced significant results for the U.S. Army and other agencies interested in monitoring off-road vehicular damage. An indication of the spatial resolution and types of remote sensor systems needed for best detecting off-road vehicular damage has been provided. It has also provided the information necessary to adequately and efficiently enhance this imagery for optimal detection of off-road vehicular damage.

This research has also produced significant results in documenting differences in classification accuracy as a function of remote sensor system spatial resolution and the spatial characteristics of the cover types involved. It has been shown that higher spatial resolution sensor systems are not always best for detecting and monitoring vegetative cover types. In addition, differences in spectral variation from pixel to pixel for different vegetative cover types has been documented. This helps explain the differences in classification accuracy observed for the different sensor systems and cover types involved. A brief synopsis of the significant results obtained in this research are provided in this chapter.

- Off-road vehicular damage was best enhanced using a weighted Laplacian filter, and this type of filter was the most time efficient.

In 6 out of 9 data sets, the technique that best enhanced the imagery for detection of tank trails were weighted Laplacian filters. Specifically, the weighted Laplacian filter that produced the best enhancement of off-road vehicular damage was:

0	-1	0
-1	5	-1
0	-1	0

Therefore, for agencies interested in monitoring off-road vehicular damage using remote sensor digital data, the weighted Laplacian filter above will produce the optimum results.

- The enhancement of Geoscan's MKII Airborne Multispectral Scanner data having 6.5 meter spatial resolution to detect off-road vehicular damage provided the best results when compared to other remote sensor digital data used in this research.

Eleven out of eleven interpreters selected Geoscan's MKII Airborne Multispectral Scanner, using the first three principal component bands derived from every portion of the electromagnetic spectrum, as the best enhanced image for detecting tank trails. A statistical evaluation of this result indicated that more than 72% of all interpreters would

select this image 95 times out of 100. Additionally, 8 out of 11 interpreters selected the one-band image, from the Airborne Scanner as the second best enhanced image for detecting tank trails. Selection of these two images as first and second best over all data sets was not due to chance occurrence (α = .001).

- Traditional photointerpretation techniques of high-quality aerial photography such as provided by the National Aerial Photography Program (NAPP) will provide more information regarding off-road vehicular damage than remote sensor digital data.

Standard NAPP color-infrared aerial photography was carefully examined using traditional photointerpretation techniques within a portion of the study area to determine the number of tank trails that were resolved by the aerial photography. In addition, the number of tank trails visible in the best enhanced image of remote sensor digital data was determined. The actual number of tank trails visible in the digital imagery was only 65-70% of the total number visible in the NAPP aerial photography. Most of the detail that was lost in the digital imagery were small tank trails, i.e., those that had been travelled on a very limited number of times.

- A classification of remote sensor data that included a Normalized Difference Vegetation Index (NDVI) produced misleading and false information regarding the amount of vegetation present in different locations. The amount of

vegetation present on dark-colored soils was overestimated. It was underestimated on light-colored soils.

An evaluation was conducted to determine whether NDVI would aid in classifying vegetation at Pinon Canyon (see Section 3.4.1). Study Area 1 from the Airborne Scanner data was first classified using the three principal component bands and the NDVI band. A second data set was then created using only the three principal component bands. The two classifications were then compared. A test area containing 172 pixels that consisted of a very light-colored soil with 10-20% vegetative cover was selected to test the classification on light-colored soil. Another test area containing 242 pixels that consisted of a very dark-colored shale with nearly no vegetation present was selected to test the classification on dark colored soil.

The classification of the light-colored soil area using the NDVI band classified 50 pixels as vegetation and 122 pixels as roads/exposed soil. The classification without NDVI, however, classified 101 pixels as vegetation and 71 pixels as roads/exposed soil. The estimate of vegetation present in the classification using the NDVI band was lower than was actually present in this location. The classification without the NDVI band more accurately reflected the amount of vegetation present in this test area.

The classification of dark-colored soil using the NDVI band classified 168 pixels as vegetation and 104 pixels as dark shale. The classification without NDVI, however,

classified 2 pixels as vegetation and 240 pixels as dark shale. The estimate of vegetation present in the classification using the NDVI band was higher than was actually present in this location. The classification without the NDVI band more accurately reflected the amount of vegetation present in this test area.

A visual, qualitative evaluation of the two classifications was also done in these test areas. Using the NDVI band in the classification procedure resulted in an underestimate of vegetation in light-colored soils, and an overestimate of vegetation in dark-colored soils.

In summary, since the classification that contained the NDVI band produced an underestimation and overestimation of vegetation in light-colored and dark-colored soil respectively, it was not included in the final classification procedure.

- Overall classification accuracy for the individual cover type classes for the Airborne Scanner was 74.9% as compared to 78.5% for Landsat Thematic Mapper.

These results are based on the assumption that the locations digitized as test polygons in the classified image accurately reflect the information within the selected test locations (LCTA plots, etc.). The results demonstrate that a relatively high overall classification accuracy can be achieved for very specific land use and land cover categories, based primarily on species, vegetation density (for grass

cover types), and percent crown closure (for forest cover types). These results are obtainable in a mixed rangeland environment by sensors of varying spatial resolution.

- Overall classification accuracy for the major cover type groups for Geoscan's MKII Airborne Multispectral Scanner was 85% as compared to 91% for Landsat Thematic Mapper.

When the individual categories were combined into major cover type groups (i.e., forest, grass, and roads/exposed soil), an increase of 10% and 12% were observed for the Airborne Scanner and Landsat TM, respectively. This indicates that many of the pixels that were misclassified were actually classified in other individual classes contained within the same major cover type group (i.e., errors were occurring between categories that differed only in vegetation density or percent crown closure). By combining the individual classes into major cover type groups, the minimum level of accuracy for Level I land use and land cover categories of 85% has been achieved (U.S. Department of the Interior, 1976).

- There were no significant differences in classification accuracy between classifications of individual cover types obtained using Geoscan's MKII Airborne Multispectral Scanner and Landsat Thematic Mapper when all cover types were considered (α = .01). There was also no significant difference in the classification accuracies between the data sets when only grass cover types were considered (α =

.01). There were, however, significant differences in classification accuracy between the two data sets for the forest and roads/exposed soil cover types when they were considered separately (α = .01).

A procedure was conducted that evaluated the differences in the percent of correctly classified pixels for individual test area for the classifications of Landsat TM and the Airborne Scanner data using the student's t-test (see Section 4.2.1 and 4.2.2). Based on these differences in the percent of correctly classified pixels for each test area and the results of the student's t-test, no significant difference was found in classification accuracy between Landsat TM and the Airborne Scanner when the differences from all test areas were considered (α = .01).

However, when the differences for forest test areas were considered, a significant difference was observed (α = .01). The percent of correctly classified pixels from the Landsat TM classification was subtracted from the percent of correctly classified pixels from the Airborne Scanner. In the case of forest cover types, the differences observed were all negative. Thus, the percent of correctly classified pixels was higher in the classification produced from Landsat TM data for forest cover types. Therefore, the classification of forest cover types was significantly higher in Landsat TM as compared to the Airborne Scanner. This result is primarily due to the high spectral variability from pixel to pixel that occurs in forest cover types (see Section 4.3). The reason

that Landsat TM achieved a higher classification accuracy for forest cover types is a function of the lower spatial resolution (larger pixel size) of Landsat Thematic Mapper. The larger pixel is able to average much of the spectral variation that occurs in cover types such as a forest canopy. On the other hand, because of the high spatial resolution of certain sensor systems such as the Airborne Scanner used in this research, the high spectral variability that is a natural phenomena of many cover types (i.e., forests) is recorded on a pixel by pixel basis in remotely sensed digital imagery. This spectral variability from pixel to pixel in the data results in poor classification results for these cover types.

When the differences for roads/exposed soil test areas were considered, a significant difference was also observed (α = .01). In the case of roads/exposed soil test areas, however, the differences observed were all positive. This means that the classification produced from the Airborne Scanner data resulted in a significantly higher classification than Landsat TM. This is primarily due to the smaller spatial resolution. More pixels are completely within the cover type, and a lower proportion are boundary pixels. This improves classification accuracy for cover types that are spectrally homogeneous and of small areal extent.

No significant differences in the percent of correctly classified pixels were found for the test areas containing grassland cover types (α = .01). This is because the spectral variability from pixel to pixel in a natural grassland cover

type is relatively low and constant (see Section 4.3). Thus, a high spatial resolution sensor will receive approximately the same information as a lower spatial resolution sensor.

The reason that there were no significant differences in classification accuracy between the two sensors when all cover types were involved is, in part, due to the fact that the differences in classification accuracy between forest cover types and the roads/exposed soil were of similar magnitude, but in opposing directions, so as to offset each other. In other words, the high accuracy in the Landsat TM classification for forest cover types was offset by the high accuracy in the Airborne Scanner classification for roads/exposed soil.

To summarize, remote sensor systems that have low spatial resolution will classify cover types of high spectral variability with a significantly higher percentage of accuracy as compared to sensor systems with a higher spatial resolution. This is because the larger pixel in the lower spatial resolution sensor is able to average the high spectral variability found in forest cover types. Additionally, areas that have low spectral variability (e.g., grassland) will be classified with approximately the same degree of accuracy, irrespective of sensor spatial resolution.

5.2 APPLICABILITY OF RESULTS

The results of this research indicate that agencies or land managers interested in detecting off-road vehicular

damage with very high spatial resolution remote sensor digital imagery should use a weighted Laplacian filter such as the one described above to enhance the imagery. Unless a very high spatial resolution sensor is available, high quality aerial photography, such as provided by the National Aerial Photography Program (NAPP), provides the best results for detecting off-road vehicular damage, particularly the damage that was created by a very limited amount of traffic (perhaps only one pass from one vehicle).

The results of this research also demonstrate that a low spatial resolution sensor such as Landsat Thematic Mapper be used to monitor overall changes in vegetation density on U.S. Army Training Maneuver Sites rather than a high spatial resolution sensor. Although classification accuracy between the two sensors will be similar in grassland communities, the accuracy of the higher (finer) spatial resolution sensor will be lower in forest cover types as compared to that of a lower (coarser) spatial resolution sensor such as Landsat TM.

5.3 RECOMMENDED TOPICS FOR FUTURE RESEARCH

Several topics could be pursued as topics for further research. As described in this research (see Section 4.1.1), a more quantitative approach in determining the actual amount of damage information recorded by a multispectral scanner is possible. This involves digitizing the vehicular damage into a raster (grid cell) geographic information system. A value of 1 would represent damaged areas, whereas a 0 would

represent non-damaged areas. The computer output would be the total number of cells that contain off-road vehicular damage.

Following the same procedure for digital imagery, a reclassification of the data would create a binary map (i.e., a value of 1 represents vehicular damage, a value of 0 represents everything else). After the total number of cells were calculated by the computer, a direct comparison of the number of cells present in aerial photography versus the digital imagery could be made.

A method that may be useful in monitoring off-road vehicular damage and the changes that occur over time is possible using aerial photography and a geographic information system (GIS). Digitizing the damage that has occurred in an area into a GIS will allow a "degree of damage" code to be applied to each damaged area. For example, a damage code could be developed where a value of 1 represented minimal damage and a value of 5 represented extreme damage. Aerial photography obtained over the same location one or two years later could provide an interesting comparison to previous damage. The damaged areas could again be digitized with appropriate damage codes applied to each damaged area. A comparison between the two dates could then be made to see what changes have occurred since the first set of photography was obtained. Types of changes may be: 1) new damage, 2) increased "degree of damage", 3) decreased "degree of damage" (i.e., recovery has taken place), or 4) no change has occurred. This type of information would be very useful for

a land manager attempting to develop or adjust a land use plan for continued use of our natural resources.

A very efficient method for comparing the information from the two dates is available. An overlay procedure within a GIS could overlay the two map layers, thus providing information regarding the coincidence of the tank trails. A major drawback of this procedure, however, is that if the two images are shifted by just one pixel (i.e., poor alignment), the statistical evaluation of coincidence will be much lower than if the two images were precisely registered to each other.

A method to determine what the alignment is between the two data sets is also available. Using the GIS to construct concentric rings around each tank trail in one data set would determine how far away each cell was from the closest tank trail. Overlaying this new map onto the second data set would provide spatial statistical information regarding the degree of misalignment between the two data sets.

Another area for potential future research could involve a comparison of higher spatial resolution multispectral imagery to determine what resolution is needed to detect all of the damage caused by off-road vehicles. This data may be obtained by an airborne multispectral scanner flown at varying altitudes, thus producing different spatial resolution data. Additionally, investigations into the utility of the Airborne Visible-Infrared Imaging Spectrometer (AVIRIS) or High Resolution Imaging Spectrometer (HIRIS) would be useful.

A Fourier transformation applied to the data sets may be a useful tool for extracting tank trail information such as the number of trails and the angles between them. This is another potential for future research.

Exploring the advantages and limitations of a flatbed or drum scanner to digitize aerial photography to extract information about off-road vehicular damage is proposed as another topic for further research. A visual, qualitative evaluation of the NAPP aerial photography used in this research reveals many details that were lost due to the video digitization process. A comparison of the scanned aerial photography and other remote sensor systems would be very interesting.

REFERENCES CITED

Acevedo, W., J.S. Buis, and R.C. Wrigley. "Changes in Classification Accuracy Due to Varying Thematic Mapper and Multispectral Scanner Spatial, Spectral, and Radiometric Resolution." In International Symposium on Remote Sensing of Environment: Proceedings of the 18th International Symposium Paris, France, October 1-5, 1984, by Environmental Research Institute of Michigan and National d'Etudes Spatiales (CNES). Ann Arbor, Michigan: Environmental Research Institute of Michigan, 1984, 27-44.

Badhwar, G.D., K.E. Henderson, D.E. Pitts, K.R. Johnson, M.L. Sestak, T. Woolford, and J. Carnes, 1984. "Comparison of Simulated Thematic Mapper Data and Multispectral Scanner Data," Remote Sensing of Environment, 14:247-255.

Benjamin, Susan, and Leonard Gaydos, 1990. "Spatial Resolution Requirements for Automated Cartographic Road Extraction," Photogrammetric Engineering and Remote Sensing, 56(1):93-100.

Berthod, Marc and Mary Aline Serendero. "Extraction of Thin Networks on Satellite Imagery." In 9th International Conference on Pattern Recognition in Rome, Italy, November 14-17, 1988, by the International Association for Pattern Recognition. New York: IEEE Computer Society press, 1988, 456-458.

Chavez, Pat S., Jr., and Brian Bauer, 1982. "An Automatic Optimum Kernel-Size Selection Technique for Edge Enhancement," Remote Sensing of Environment, 12:23-38.

Chavez, Pat S., Jr., and Andrew Yaw Kwarteng, 1989. "Extracting Spectral Contrast in Landsat Thematic Mapper Data Using Selective Principal Component Analysis," Photogrammetric Engineering and Remote Sensing, 55(3):339-348.

Chen, Ling-Hwei, and Wen-Hsiang Tsai, 1988. "Moment-Preserving Line Detection," Pattern Recognition, 21(1):45-53.

Chittineni, C.B., 1983. "Edge and Line Detection in Multidimensional Noisy Imagery Data," IEEE Transactions

on Geoscience and Remote Sensing, GE-21(2):163-174.

Clark, Jerry and Nevin A. Bryant. "Landsat-D Thematic Mapper Simulation Using Aircraft Multispectral Scanner Data." In International Symposium on Remote Sensing of Environment: Proceedings of the 11th International Symposium in Ann Arbor, Michigan, 25-29 April, 1977, by Environmental Research Institute of Michigan. Ann Arbor, Michigan: Environmental Research Institute of Michigan, 1977, 483-491.

Curran, Paul J., and H. Dawn Williamson, 1988. "Selection a Spatial Resolution for Estimation of Per-Field Green Leaf Area Index," International Journal of Remote Sensing, 9(7):1243-1250.

Davis, Larry S., 1975. "A Survey of Edge Detection Techniques," Computer Graphics and Image Processing, 4:248-270.

Diersing, Victor E., Robert B. Shaw, Steven D. Warren, and Edward W. Novak, 1988. "A User's Guide for Estimating Allowable Use of Tracked Vehicles on Nonwooded Military Training Lands," Journal of Soil and Water Conservation, March-April 1988, pp. 191-195.

Diersing, Victor E., Steven D. Warren, Robert B. Shaw, David J. Tazik, and Robert J. Brozka, 1989. U.S. Army Land Condition Trend Analysis (LCTA) Field Methods (Draft).

Duda, Richard O., and Peter E. Hart. Pattern Classification and Scene Analysis. New York, London, Sydney, and Toronto: John Wiley & Sons, 1973.

Eberlein, R.B., and J.S. Weszka, 1975. "Mixtures of Derivative Operators as Edge Detectors," Computer Graphics and Image Processing, 4:180-183.

ERDAS, Inc. Earth Resources Data Analysis System, Inc., 2801 Buford Highway, Suite 300, Atlanta, Georgia, U.S.A. 30329. Tel: (404) 248-9000.

Fleming, Michael D., and Roger M. Hoffer. "Computer-Aided Analysis Techniques for an Operational System to Map Forest Lands Utilizing Landsat MSS Data." M.S. Thesis, Purdue University, 1977.

Ford, Gary E., V. Ralph Algazi, and Doreen I. Meyer, 1983. "A Noninteractive Procedure for Land-Use Determination," Remote Sensing of Environment, 13:1-16.

Gil, Baldemar, Amar Mitiche, and J.K. Aggarwal, 1983. "Experiments in Combining Intensity and Range Edge Maps,"

Computer Vision, Graphics, and Image Processing, 21:395-411.

Goodwin, W., 1977. "Off-road vehicle use and erosion at Holister Hills Park," Southern California Academy of Sciences, Annual meeting Abstracts.

Goran, W.D., L.L. Radke, and W.D. Severinghaus, 1983. "An Overview of the Ecological Effects of Tracked Vehicles on Major U.S. Army Installations," Technical Report N-140. Construction Engineering Research Laboratory, Champaign, Illinois, 1983.

Graetz, R.D., and R.P. Pech, 1987. "Detecting and Monitoring Impacts of Ecological Importance in Remote Arid Lands: A Case Study in the Southern Simpson Desert of South Australia," Journal of Arid Environments, 12:269-284.

Green, A.J., D.D. Randolf, and A.A. Rula, 1973. "The Effect of Military Transportation Activities on the Environment," Miscellaneous Paper M-73-15, Waterways Experiment Station, Vicksburg, Mississippi, 1973.

Haack, Barry, Nevin Bryant, and Steven Adams, 1987. "An Assessment of Landsat MSS and TM Data for Urban and Near-Urban Land-Cover Digital Classification," Remote Sensing of Environment, 21:201-213.

Hord, R.M. Digital Image Processing of Remotely Sensed Data. New York: Academic Press, 1982.

Huete, A.R., and R.D. Jackson, 1987. "Suitability of Spectral Indices for Evaluating Vegetation Characteristics on Arid Rangelands," Remote Sensing of Environment, 23:213-232.

Irons, James R., and Ruth L. Kennard, 1986. "The Utility of Thematic Mapper Sensor Characteristics for Surface Mine Monitoring," Photogrammetric Engineering and Remote Sensing, 52(3):389-396.

Irons, J.R., B.L. Markham, R.F. Nelson, D.L. Toll, D.L. Williams, R.S. Latty, R.L. Kennard, and M.L. Stauffer. "The Effects of Sensor Advancements on Thematic Mapper Data Classification." In International Symposium on Remote Sensing of Environment: Proceedings of the Symposium in Paris, France, October 1-5, 1984, by Environmental Research Institute of Michigan and National d'Etudes Spatiales (CNES). Ann Arbor, Michigan: Environmental Research Institute of Michigan, 1984, 1759-1773.

Iverson, Richard M., Bern S. Hinkley, Robert M. Webb, and Bernard Hallet, 1981. "Physical Effects of Vehicular

Disturbances on Arid Landscapes," Science, 212:915-917.

Jensen, John R. Introductory Digital Image Processing A Remote Sensing Perspective. Englewood Cliffs, N.J.: Prentice-Hall, 1986.

Johnson, Lee F., Nevin A. Bryant, Anthony J. Brazel, Charles F. Hutchinson, and Robert C. Balling. "Using Remotely Sensed Data to Monitor Land Surface Climatology Variations in a Semi-arid Grassland." International Geoscience and Remote Sensing Symposium (IGARSS): Proceedings of the Symposium in Vancouver, Canada, July 10-14, 1989, by The Institute of Electrical and Electronic Engineers, Inc., and Canadian Remote Sensing Society. Vancouver: IGARSS '89 12th Canadian Symposium on Remote Sensing, 1989, 184-187.

Kan, E.P., D.L. Ball, J.P. Basu, and R.L. Smelser. "Data Resolution Versus Forestry Classification and Modeling." In Machine Processing of Remotely Sensed Data: Proceedings of the Symposium in West Lafayette, Indiana, June 3-5, 1975, by Purdue University. New York: The Institute of Electrical and Electronic Engineers, Inc., 1975, 1b-24 - 1b-36.

Kirsch, R., 1971. "Computer Determination of the Constituent Structure of Biological Images," Computers and Biomedical Research, 4:315-328.

Krahe, Jaime Lopez, and Pascale Pousset. "The Detection of Parallel Straight Lines with the Application of the Hough Transform." In 9th International Conference on Pattern Recognition in Rome, Italy, November 14-17, 1988, by the International Association for Pattern Recognition. New York: IEEE Computer Society press, 1988, 939-941.

Kundu, Amlan. "Robust Edge Detection." In IEEE Computer Vision & Pattern Recognition: Proceedings of the Symposium in San Diego, California, June 4-8, 1989, by IEEE Computer Society Press. Washington: Computer Society Press, 1989, 11-18.

Landgrebe, David A., Larry L. Biehl, and William R. Simmons, 1977. "An Empirical Study of Scanner System Parameters," IEEE Transactions on Geoscience Electronics, GE-15(3):120-130.

Latty, Richard S., and Roger M. Hoffer. "Computer-Based Classification Accuracy Due to the Spatial Resolution Using Per-Point Versus Per-Field classification Techniques." In Machine Processing of Remotely Sensed Data: Proceedings of the Symposium in West Lafayette, Indiana, June 23-26, 1981, by Purdue University. West

Lafayette: Purdue Research Foundation, 1981, 384-392.

Latty, R.S., R. Nelson, B. Markham, D. Williams, D. Toll, and J. Irons, 1985. "Performance Comparisons Between Information Extraction Techniques Using Variable Spatial Resolution Data," Photogrammetric Engineering and Remote Sensing, 51(9):1459-1470.

Lee, Heungju, and Kyusung Lee, 1990. ERD2MP (unpublished) software package (in development). Fort Collins, Colorado 80523

Lenz, Reiner, 1987. "Optimal Filters for the Detection of Linear Patterns in 2-D and Higher Dimensional Images," Pattern Recognition, 20(2):163-172.

Lillesand, Thomas M., and Ralph W. Kiefer. Remote Sensing and Image Interpretation. 2d ed. New York, Chichester, Brisbane, Toronto, Singapore: John Wiley & Sons, 1987.

Markham, B.L., and J.R.G. Townshend. "Land Cover Classification Accuracy as a Function of Sensor Spatial Resolution." In International Symposium on Remote Sensing of Environment: Proceedings of the Symposium in Ann Arbor, Michigan, May, 11-15, 1981, by Environmental Research Institute of Michigan. Ann Arbor: Environmental Research Institute of Michigan, 1981, 1075-1090.

Mero L., and Z. Vassy. "A Simplified and Fast Version of the Hueckel Operator for Finding Optimal Edges in Pictures." In Artificial Intelligence: Proceedings of the 4th International Conference in Tbilisi, USSR, September, 1975, 650-655.

MICROPIPS.EGA, An Advanced Image Processing System for the IBM-PC Microcomputer, by the Telesys Group, Inc., Suite 400, 5455 Wingborne Court, Columbia, Maryland 21045.

Morgenstern, James P., Richard F. Nalepka and Jon D. Erickson. "Investigation of thematic Mapper Spatial, Radiometric, and Spectral Resolution." In International Symposium on Remote Sensing of Environment: Proceedings of the 11th International Symposium in Ann Arbor, Michigan, May 25-29, 1977, by Environmental Research Institute of Michigan. Ann Arbor: Environmental Research Institute of Michigan, 1977, 693-701.

Park, Nancy F., Gary W. Petersen, and George M. Baumer, 1987. "High Resolution Remote Sensing of Spatially and Spectrally Complex Coal Surface Mines of Central Pennsylvania: A Comparison Between Simulated SPOT MSS and Landsat-5 Thematic Mapper," Photogrammetric Engineering and Remote Sensing, 53(4):415-420.

Petersen, G.W., K.F. Connors, D.A. Miller, R.L. Day, and T.W. Gardner, 1987. "Aircraft and Satellite Remote Sensing of Desert Soils and Landscapes," Remote Sensing of Environment, 23:253-271.

Pitts, David E., and Gautam Badhwar, 1980. "Field Size, Length, and Width Distributions Based on LACIE Ground Truth Data," Remote Sensing of Environment, 10:201-213.

Prewitt, J.M.S. "Object Enhancement and Extraction." In Picture Processing and Psychopictorics, edited by B.S. Lipkin and A. Rosenfeld, 75-149. New York: Academic Press, 1970.

Prose, Doug V., 1985. "Persisting Effects of Armored Military Maneuvers on Some Soils of the Mojave Desert," Environmental Geology and Water Science, 7(3):163-170.

Ribanszky, Susan, Steven D. Warren, and Mark O. Johnson (unpublished), 1990. "The Use of Satellite Imagery and Geographic Information Systems for the Selection and Monitoring of Land Condition Inventory Sites," U.S. Army Construction Engineering Research Laboratory, Environmental Division, Champaign, Illinois 61824.

Roberts, L. G. "Machine Perception of Three Dimensional Solids." In Optical and Electro-Optical Information Processing, edited by J. Tippett, D. Berkowitz, L. Clapp, C. Koester, and A. Vanderburgh, 159-197. Cambridge: Massachusetts Institute of Technology Press, 1965.

Robinson, Guner S., 1977. "Edge Detection by Compass Gradient Masks," Computer Graphics and Image Processing, 6:492-501.

Rosenfeld, Azriel, and Avinash C. Kak. Digital Picture Processing. New York, San Francisco, and London: Academic Press, 1976

Schwarz, David E., David S. Simonett, George F. Jenks, and John R. Ratzlaff, 1969. "The Construction of Thematic Land Use Maps with Spacecraft Photography," Appendix 1 of the Second Annual Report, Center for Research in Engineering Science, University of Kansas, Lawrence, USGS Contract No. 14-08-0001-10848.

Sadowski, F.G., W.A. Malila, J.E. Sarno, and R.F. Nalepka. "The Influence of Multispectral Scanner Spatial Resolution on Forest Feature Classification." In International Symposium of Remote Sensing of Environment: Proceedings of the 11th International Symposium in Ann Arbor, Michigan, May 25-29, 1977, by Environmental Research Institute of Michigan. Ann Arbor: Environmental

Research Institute of Michigan, 1977, 1279-1288.

Shaw, Gilbert B., 1979. "Local and Regional Edge Detectors: Some Comparisons," Computer Graphics and Image Processing, 9:135-149.

Shaw, R.B., S.L. Anderson, K.A. Schulz, V.E. Viersing. Plant Communities, Ecological Checklist, and Species List for the U.S. Army Pinon Canyon Maneuver Site, Colorado. Science Series No. 37. Colorado State University: Department of Range Science, 1989.

Shaw, Robert B., and Victor E. Diersing, 1989. "Allowable Use Estimates for Tracked Vehicular Training on Pinon Canyon Maneuver Site, Colorado, USA," Environmental Management, 13(6):773-782.

Shaw, Robert B., and Victor E. Diersing, 1989. "Evaluation of the Effects of Military Training on Vegetation in Southeastern Colorado," Headwaters Hydrology, June 1989, pp. 223-231.

Shaw R.B., and V.E. Diersing, 1990. "Tracked Vehicle Impacts on Vegetation at the Pinon Canyon Maneuver Site, Colorado," Journal of Environmental Quality, 19(2):234-243.

Simonett, D.S., and J.C. Coiner. "Susceptibility of Environments to Low Resolution Imaging for Land-Use Mapping." In International Symposium on Remote Sensing of Environment: Proceedings of the 7th International Symposium in Ann Arbor, Michigan, 17-21 May, 1973, by Environmental Research Institute of Michigan. Ann Arbor, Michigan: Environmental Research Institute of Michigan, 1971, 373-394.

Story, Michael, and Russell G. Congalton, 1986. "Accuracy Assessment: A User's Perspective," Photogrammetric Engineering and Remote Sensing, 52(3):397-399.

Sullivan, Gerry, Lorne Trottier, Bernard Saitta, and Carmine Iannuzzi, 1984. "Multibus Image Processor Supports 512 x 512 Displays," Electronic Imaging, October:42-47.

Thomson, F.J., J.D. Erickson, K. Koerber, and M.J. Harnage. "A Thematic mapper Performance Optimization Study." In International Symposium on Remote Sensing of Environment: Proceedings of the 10th International Symposium in Ann Arbor, Michigan, October 6-10, 1975, by Environmental Research Institute of Michigan. Ann Arbor: Environmental Research Institute of Michigan, 1975, 85-98.

Tueller, Paul T., 1987. "Remote Sensing Science applications

in Arid Environments," Remote Sensing of Environment, 23:143-154.

Tueller, Paul T., 1989. "Remote Sensing Technology for Rangeland Management Applications," Journal of Range Management, 42(6):442-453.

Tuttle, Martitia, and Gary Griggs, 1987. "Soil Erosion and Management Recommendations at Three State Vehicular Recreation Areas, California," Environmental Geology and Water Science, 10(2):111-123.

U.S. Congress. 1976. Federal Land Policy and Management Act of 1976, as amended. 94 Public Law 579, 90 Stat 2747, 43 U.S. Code 1701 et seq.

U.S. Department of the Interior. Geological Survey. Disturbance of Soil and Vegetation by the Johnson Valley-Parker Motorcycle Race of October 8, 1983, in Wilderness Study Area 304A, California and Vicinity, by H.G. Wilshire. Open-file report, U.S. Geological Survey, 84-277. U.S. Geological Survey, 1984.

U.S. Department of the Interior. Geological Survey. A Land Use and Land Cover Classification System for Use with Remote Sensor Data, by James R. Anderson, Ernest E. Hardy, John T. Roach, and Richard E. Witmer. U.S. Geological Survey Professional Paper 964. Washington, D.C.: U.S. Government Printing Office, 1976.

U.S. Department of the Interior. Geological Survey. Study Results of 9 Sites Used by Off-road Vehicles that Illustrate Land Modifications, by H.G. Wilshire. Open-file report, U.S. Geological Survey, 77-601. U.S. Geological Survey, 1977.

Vanderbrug, G.J., 1976. "Line Detection in Satellite Imagery," IEEE Transactions on Geoscience Electronics, GE-14(1):37-44.

Verma, M.R., A.K. Majumdar, and B. Chatterjee, 1987. "Edge Detection in Fingerprints," Pattern Recognition, 20(5):513-523.

Warren, P.L., and C.F. Hutchinson, 1984. "Indicators of Rangeland Change and their Potential for Remote Sensing," Journal of Arid Environments, 7:107-126.

Webb, R.H., and H.G. Wilshire. Environmental Effects of off-road vehicles. New York, N.Y.: Springer-Verlag, 1983.

Williams, Darrel L., James R. Irons, Brian L. Markham, Ross F. Nelson, David L. Toll, Richard S. Latty, and Mark L.

Stauffer, 1984. "A Statistical Evaluation of the Advantages of Landsat Thematic Mapper Data in Comparison to Multispectral Scanner Data," IEEE Transactions on Geoscience and Remote Sensing, GE-22(3):294-301.

Woodcock, Curtis E., and Alan H. Strahler, 1987. "The Factor of Scale in Remote Sensing," Remote Sensing of Environment, 21:311-332.

Zar, Jerrold H. Biostatistical Analysis. 2d Ed. Englewood Cliffs, N.J.: Prentice Hall, Inc., 1984.

APPENDICES

APPENDIX 1

Table A1.1. Land Condition Trend Analysis (LCTA) Plot information.

PLOT	COVER TYPE[3]	UTM COORDINATES	% COVER[4]
10	AGSM/HIJA/SIHY	584100-E 4142500-N	4%
11	BOGR/HIJA	583300-E 4141100-N	25%
13	BOGR/HIJA	587500-E 4140600-N	41%
14	BOGR/HIJA	588300-E 4143100-N	17%
15	SPAI/HIJA/AGSM	597400-E 4161100-N	44%
21*	BOGR/HIJA	591800-E 4147300-N	40%
22*	BOGR/BOHI	596100-E 4144900-N	31%
103	BOGR/HIJA/AGSM	595200-E 4146500-N	22%
118	BOGR/HIJA	595700-E 4151200-N	30%
124	BOGR/HIJA	597700-E 4147800-N	6%
125	BOGR/HIJA/AGSM	597500-E 4149300-N	32%

[3]Appendix 2 contains a partial listing of vegetation found at Pinon Canyon, including abbreviations used (Shaw et al 1989).

[4]Percent cover is determined by field crews. Each 6 x 100 meter plot is divided into 1-meter intervals along a line inside the plot that parallels its long axis. The plant species at each 1-meter interval are then determined. The total number of plants encountered along this line represents the average percent ground cover.

PLOT #	COVER TYPE	UTM COORDINATES	% COVER
126*	BOGR/HIJA	598100-E 4148800-N	12%
127	BOGR/HIJA/AGSM	598300-E 4150400-N	23%
128*	BOGR/HIJA	594500-E 4148800-N	20%
129*	BOGR/LICHEN	594600-E 4149700-N	45%
140*	AGSM/BOGR	595200-E 4150500-N	26%
141*	BOGR	594700-E 4147400-N	6%
143*	BOGR/HIJA/AGSM	593200-E 4145900-N	24%
144*	BOGR/HIJA	590500-E 4140500-N	19%
145	BOGR/HIJA	589800-E 4140400-N	27%
146	BOGR/HIJA	589300-E 4140500-N	14%
147*	BOGR/HIJA	588600-E 4140600-N	35%
154	HIJA/AGSM	584100-E 4142700-N	17%
156*	BOGR/HIJA	582700-E 4141100-N	22%
160*	BOGR/LICHEN	588700-E 4141100-N	41%
161	BOGR/HIJA	588300-E 4141800-N	40%
163*	BOGR/LICHEN	586900-E 4141200-N	47%
164	BOGR/HIJA	589000-E 4144800-N	17%
192	BOGR/HIJA	586500-E 4137400-N	35%
203*	BOGR/HIJA	587600-E 4144100-N	19%

APPENDIX 2

Table A2.1. A partial list of dominant vegetation found at Pinon Canyon.

ABBREVIATION[5]	SCIENTIFIC NAME	COMMON NAME
BOGR	Bouteloua gracilis	Blue grama
HIJA	Hilaria jamesii	Galleta
AGSM	Agropyron smithii	Western wheatgrass
SPAI	Sporobolus airoides	Alkali sacaton
BOER	Bouteloua eriopoda	Black grama
JUMO	Juniperus monosperma	One-seeded juniper
GLME	Glossopetalon meionandra	Greasebush
OPIM	Opuntia imbricata	Tree cholla
SIHY	Sitanion hystrix	Squirreltail
SAIB	Salsola iberica	Russian thistle
TAPE	Tamarix pentandra	Five-stamen tamarix
PIED	Pinus edulis	Pinyon pine

[5] Abbreviations are made by using the first two letters from each scientific name. A combination of four letters is thus made.

APPENDIX 3

EDGE AND LINE ENHANCEMENT TECHNIQUES USED*

1. Laplacian (zero-weight) filters.[6]

0	-1	0
-1	4	-1
0	-1	0

0	-.5	0
-.5	2	-.5
0	-.5	0

0	-.25	0
-.25	1	-.25
0	-.25	0

0	-2	0
-2	8	-2
0	-2	0

-1	-1	-1
-1	8	-1
-1	-1	-1

0	-1.75	0
-1.75	7	-1.75
0	-1.75	0

0	-.75	0
-.75	3	-.75
0	-.75	0

-.5	-.5	-.5
-.5	4	-.5
-.5	-.5	-.5

0	-1.25	0
-1.25	5	-1.25
0	-1.25	0

0	-1.5	0
-1.5	6	-1.5
0	-1.5	0

1	-2	1
-2	4	-2
1	-2	1

-.75	-.75	-.75
-.75	6	-.75
-.75	-.75	-.75

2	-4	2
-4	8	-4
2	-4	2

0.5	-1	0.5
-1	2	-1
0.5	-1	0.5

-.25	-.25	-.25
-.25	2	-.25
-.25	-.25	-.25

1.5	-3	1.5
-3	6	-3
1.5	-3	1.5

*Filters bordered by double lines were best for a particular method.

[6]In this research, Laplacian and Bi-Laplacian edge detectors are grouped together within zero-weight and weighted filters.

2. Laplacian (weighted) filters.

0	-1	0
-1	5	-1
0	-1	0

0	-1.5	0
-1.5	7	-1.5
0	-1.5	0

0	-2	0
-2	9	-2
0	-2	0

1	-2	1
-2	5	-2
1	-2	1

0	-1	0
-1	3	-1
0	-1	0

3. Sobel Edge Enhancement. (Image = $(X^2 + Y^2)^{1/2}$)

X Components:

-1	0	1
-2	0	2
-1	0	1

-.5	0	.5
-1	0	1
-.5	0	.5

-2	-1	0
-1	0	1
0	1	2

-4	-2	0
-2	0	2
0	2	4

-2	-1	0
-1	0	1
0	1	2

Y Components:

1	2	1
0	0	0
-1	-2	-1

.5	1	.5
0	0	0
-.5	-1	-.5

0	1	2
-1	0	1
-2	-1	0

0	2	4
-2	0	2
-4	-2	0

2	1	0
1	0	-1
0	-1	-2

2	1	.5
1	0	-1
.5	-1	-2

-2	-1	.5
-1	0	1
.5	1	2

2	1	.5
1	0	-1
.5	-1	-2

.5	1	2
-1	0	1
-2	-1	.5

4. High-pass filters (3 x 3 window).

-1	-1	-1
-1	9	-1
-1	-1	-1

-1	-1	-1
-1	17	-1
-1	-1	-1

5. Filters using a 5 x 5 window.

0	-1	-2	-1	0
-1	-2	-4	-2	-1
-2	-4	40	-4	-2
-1	-2	-4	-2	-1
0	-1	-2	-1	0

0	-1	-2	-1	0
-1	-2	-4	-2	-1
-2	-4	41	-4	-2
-1	-2	-4	-2	-1
0	-1	-2	-1	0

-.3	-.3	-.3	-.3	-.3
-.3	-.3	-.3	-.3	-.3
-.3	-.3	9.7	-.3	-.3
-.3	-.3	-.3	-.3	-.3
-.3	-.3	-.3	-.3	-.3

-1	-1	-1	-1	-1
-1	-1	-1	-1	-1
-1	-1	24	-1	-1
-1	-1	-1	-1	-1
-1	-1	-1	-1	-1

-1	-1	-1	-1	-1
-1	-1	-1	-1	-1
-1	-1	25	-1	-1
-1	-1	-1	-1	-1
-1	-1	-1	-1	-1

6. Low-pass filter (In addition to the 3 x 3 unity filter below, a 5 x 5 unity filter was also tested).

1	1	1
1	1	1
1	1	1

7. Robert's edge detector.

i,j	i,j+1
i+1,j	i+1,j+1

Image = [abs((i,j) - (i+1,j+1)) + abs((i,j+1) - (i+1,j))]

Where abs refers to the absolute value.

8. Prewitt directional filters, first individually, then combined into one image by simple addition.

North:

1	1	1
1	-2	1
-1	-1	-1

Northeast:

1	1	1
-1	-2	1
-1	-1	1

East:

-1	1	1
-1	-2	1
-1	1	1

Southeast:

-1	-1	1
-1	-2	1
1	1	1

South:

-1	-1	-1
1	-2	1
1	1	1

Southwest:

1	-1	-1
1	-2	-1
1	1	1

West:

1	1	-1
1	-2	-1
1	1	-1

Northwest:

1	1	1
1	-2	-1
1	-1	-1

9. Kirsch gradient filters.

5	5	5
-3	0	-3
-3	-3	-3

5	5	-3
5	0	-3
-3	-3	-3

5	-3	-3
5	0	-3
5	-3	-3

-3	-3	-3
5	0	-3
5	5	-3

-3	-3	-3
-3	0	-3
5	5	5

-3	-3	-3
-3	0	5
-3	5	5

-3	-3	5
-3	0	5
-3	-3	5

-3	5	5
-3	0	5
-3	-3	-3

10. Prewitt three-level simple filters.

1	1	1
0	0	0
-1	-1	-1

1	1	0
1	0	-1
0	-1	-1

1	0	-1
1	0	-1
1	0	-1

0	-1	-1
1	0	-1
1	1	0

-1	-1	-1
0	0	0
1	1	1

-1	-1	0
-1	0	1
0	1	1

-1	0	1
-1	0	1
-1	0	1

0	1	1
-1	0	1
-1	-1	0

11. Prewitt five-level simple filters.

1	2	1
0	0	0
-1	-2	-1

2	1	0
1	0	-1
0	-1	-2

1	0	-1
2	0	-2
1	0	-1

0	-1	-2
1	0	-1
2	1	0

-1	-2	-1
0	0	0
1	2	1

-2	-1	0
-1	0	1
0	1	2

-1	0	1
-2	0	2
-1	0	1

0	1	2
-1	0	1
-2	-1	0

12. Mero-Vassy filter. (Image = (abs(A) + abs(B))), where abs refers to the absolute value.

A Component:

1	1
-1	-1

B Component:

-1	1
-1	1

13. Prewitt gradient filters. (Image = A + B).

A Component:

1	1	1
0	0	0
-1	-1	-1

B Component:

1	0	-1
1	0	-1
1	0	-1

14. Chittineni filters.

(Laplacian)

-1	2	-1
2	5	2
-1	2	-1

(Non-Laplacian)

1	0	-1
0	0	0
-1	0	1

1	1	1
-2	-2	-2
1	1	1

-1	-1	-1
0	0	0
1	1	1

-1	0	1
-1	0	1
-1	0	1

1	-2	1
1	-2	1
1	-2	1

Techniques 15-22:

Consider the following matrix of pixels from a hypothetical image. Each cell in the matrix may be represented as follows (the letters A-I are for convenience in referring to the cells):

$DN_{i-1,j-1}$ (A)	$DN_{i-1,j}$ (B)	$DN_{i-1,j+1}$ (C)
$DN_{i,j-1}$ (D)	$DN_{i,j}$ (E)	$DN_{i,j+1}$ (F)
$DN_{i+1,j-1}$ (G)	$DN_{i+1,j}$ (H)	$DN_{i+1,j+1}$ (I)

15. A "vertical gradient" image was obtained by performing the following equation to each pixel in the image:

$$DN_{i,j} - DN_{i-1,j} \quad (\text{or } E - B).$$

This procedure enhanced horizontal lines and edges in the imagery.

16. A "horizontal gradient" image was obtained by performing the following equation to each pixel in the image:

$$DN_{i,j} - DN_{i,j+1} \quad (\text{or } E - F).$$

This procedure enhanced vertical lines and edges in the imagery.

17. A "NW-SE (diagonal) gradient" image was obtained by performing the following equation to each pixel in the image:

$$DN_{i,j} - DN_{i-1,j-1} \quad (\text{or } E - A).$$

This procedure enhanced lines and edges oriented in a NE-SW direction.

18. A "NE-SW (diagonal) gradient" image was obtained by performing the following equation to each pixel in the image:

$$DN_{i,j} - DN_{i-1,j+1} \quad \text{(or E - C)}.$$

This procedure enhanced lines and edges oriented in a NW-SE direction.

19. Adding both the vertical and horizontal difference images above created an image with all horizontal and vertical lines and edges enhanced.

20. Adding both diagonal difference images created an image with all diagonal lines and edges enhanced.

21. Adding all difference images together created an image with lines and edges in all directions enhanced.

22. An isogradient method of enhancing both horizontal and vertical lines and edges is given by the following equation:

$$(vert^2 + horiz^2)^{1/2}$$

Where $vert^2$ is the vertical gradient image (E - B) squared, and $horiz^2$ is the horizontal gradient image (E - F) squared.

23. In addition to the methods outlined above, the original imagery was included as another "method" for evaluation.

The methods outlined above were also applied to images that were first treated using the high-pass and low-pass filters. This was performed for two reasons. First, it was speculated that a high-pass filter first applied to the imagery would enhance tank trails to a certain extent, and subsequent techniques specifically designed for edge and line enhancement would enhance them even more. Second, when the large amount of salt and pepper noise became evident in data set 4, the low-pass filter was applied to the imagery to determine if this would reduce the problems encountered with

such noise. These procedures did not aid in the enhancement of the digital imagery for tank trails.

APPENDIX 4

KOLMOGOROV-SMIRNOV GOODNESS-OF-FIT TEST FOR NORMALITY

Differences in classification accuracy as listed in Table 4.14 represent continuous data. The Kolmogorov-Smirnov goodness-of-fit test for normality was first developed for use with continuous data, and is preferable to the Chi-square goodness-of-fit test for this type of data (Zar 1984).

Four tests for normality were conducted. First, data from all general cover types were tested to determine normality for the entire data set. Second, data from each of the general cover types (i.e., forested areas, roads/exposed soil and grassland areas) were tested for normality. Tables A4.1 through A4.4 contain information used for these tests.

The Kolmogorov-Smirnov test for normality measures goodness-of-fit of the cumulative relative observed frequency (Rel F_i) of the data in question to the cumulative relative expected frequency (Rel F_i') if that data were normally distributed. As indicated on tables 1 through 4, value D_i and D_i' are calculated by taking the absolute value of the differences between F_i and F_i', and F_{i-1} and F_i' respectively. The largest value obtained in either the D_i or the D_i' column becomes a value known as D. This number is compared to the Kolmogorov-Smirnov critical value for D as found in tables in

Table A4.1. Data used for Kolmogorov-Smirnov goodness-of-fit test for normality for the differences in classification accuracy between the Airborne Scanner and Landsat TM for all major cover type groups combined.

Differences in Percent Correct Between Data Sets 4 and 8	Observed Frequency	Cumulative Observed Frequency	Cumulative Relative Obs. Freq. (Rel F_i)	Cumulative Rel. Expected Freq. (Rel F_i')	D_i $\lvert F_i - F_i' \rvert$	D_i' $\lvert F_{i-1} - F_i' \rvert$
< -60.0	0	0	0.0000	0.0032	0.0032	0.0032
(-60.0) - (-55.0)	1	1	0.0286	0.0060	0.0226	0.0060
(-55.0) - (-50.0)	1	2	0.0571	0.0110	0.0461	0.0176
(-50.0) - (-45.0)	0	2	0.0571	0.0192	0.0379	0.0379
(-45.0) - (-40.0)	0	2	0.0571	0.0314	0.0257	0.0257
(-40.0) - (-35.0)	0	2	0.0571	0.0516	0.0055	0.0055
(-35.0) - (-30.0)	0	2	0.0571	0.0793	0.0222	0.0222
(-30.0) - (-25.0)	2	4	0.1143	0.1170	0.0027	0.0599
(-25.0) - (-20.0)	2	6	0.1714	0.1660	0.0054	0.0517
(-20.0) - (-15.0)	0	6	0.1714	0.2266	0.0552	0.0552
(-15.0) - (-10.0)	3	9	0.2571	0.3015	0.0444	0.1301
(-10.0) - (- 5.0)	3	12	0.3429	0.3821	0.0392	0.1250
(- 5.0) - (0.0)	2	14	0.4000	0.4681	0.0681	0.1252
(0.0) - (5.0)	4	18	0.5143	0.5557	0.0414	0.1557
(5.0) - (10.0)	4	22	0.6286	0.6406	0.0120	0.1263
(10.0) - (15.0)	4	26	0.7429	0.7190	0.0239	0.0904
(15.0) - (20.0)	2	28	0.8000	0.7881	0.0119	0.0452
(20.0) - (25.0)	2	30	0.8571	0.8461	0.0110	0.0461
(25.0) - (30.0)	1	31	0.8857	0.8925	0.0068	0.0354
(30.0) - (35.0)	2	33	0.9429	0.9279	0.0150	0.0422
(35.0) - (40.0)	1	34	0.9714	0.9535	0.0179	0.0106
(40.0) - (45.0)	1	35	1.0000	0.9713	0.0287	0.0001
> 45.0	0	35	1.0000	1.0000	0.0000	0.0000

Table A4.2. Data used for Kolmogorov-Smirnov goodness-of-fit test for normality for the differences in classification accuracy between the Airborne Scanner and Landsat TM for forested areas.

Differences in Percent Correct for Forested Areas Between Data Sets 4 and 8	Observed Frequency	Cumulative Observed Frequency	Cumulative Relative Obs. Freq. (Rel F_i)	Cumulative Rel. Expected Freq. (Rel F_i')	D_i $\lvert F_i - F_i' \rvert$	D_i' $\lvert F_{i-1} - F_i' \rvert$
< -60.0	0	0	0.0000	0.0465	0.0465	0.0465
(-60.0) - (-50.0)	2	2	0.2857	0.1357	0.1500	0.1357
(-50.0) - (-40.0)	0	2	0.2857	0.3050	0.0193	0.0193
(-40.0) - (-30.0)	0	2	0.2857	0.5239	0.2382	0.2382
(-30.0) - (-20.0)	4	6	0.8571	0.7389	0.1182	0.4532
(-20.0) - (-10.0)	0	6	0.8571	0.8888	0.0317	0.0317
(-10.0) - (0.0)	1	7	1.0000	0.9641	0.0359	0.1070
> 0.0	0	7	1.0000	1.0000	0.0000	0.0000

Table A4.3. Data used for Kolmogorov-Smirnov goodness-of-fit test for normality for the differences in classification accuracy between the Airborne Scanner and Landsat TM for roads/exposed soil.

Differences in Percent Correct for Roads/Soil Between Data Sets 4 and 8	Observed Frequency	Cumulative Observed Frequency	Cumulative Relative Obs. Freq. (Rel F_i)	Cumulative Rel. Expected Freq. (Rel F_i')	D_i $\lvert F_i - F_i' \rvert$	D_i' $\lvert F_{i-1} - F_i' \rvert$
< 10.0	0	0	0.0000	0.0606	0.0606	0.0606
(10.0) - (20.0)	4	4	0.3636	0.2981	0.0655	0.2981
(20.0) - (30.0)	3	7	0.6364	0.6879	0.0515	0.3243
(30.0) - (40.0)	3	10	0.9091	0.9357	0.0266	0.2993
(40.0) - (50.0)	1	11	1.0000	0.9945	0.0055	0.0854
> 50.0	0	11	1.0000	1.0000	0.0000	0.0000

Table A4.4. Data used for Kolmogorov-Smirnov goodness-of-fit test for normality for the differences in classification accuracy between the Airborne Scanner and Landsat TM for grassland areas.

Differences in Percent Correct for Grassland Areas Between Data Sets 4 and 8	Observed Frequency	Cumulative Observed Frequency	Cumulative Relative Obs. Freq. (Rel F_i)	Cumulative Rel. Expected Freq. (Rel F_i')	D_i $\lvert F_i - F_i' \rvert$	D_i' $\lvert F_{i-1} - F_i' \rvert$
< -15.0	0	0	0.0000	0.0301	0.0301	0.0301
(-15.0) - (-10.0)	3	3	0.1764	0.1020	0.0744	0.1020
(-10.0) - (-5.0)	2	5	0.2941	0.2546	0.0395	0.0782
(-5.0) - (0.0)	1	6	0.3529	0.4801	0.1272	0.1860
(0.0) - (5.0)	5	11	0.6471	0.7123	0.0652	0.3594
(5.0) - (10.0)	4	15	0.8824	0.8790	0.0034	0.2319
(10.0) - (15.0)	2	17	1.0000	0.9625	0.0375	0.0801
> 15.0	0	0	1.0000	1.0000	0.0000	0.0000

statistical texts. If the calculated value of D exceeds the critical value for D as found in the statistical table, the null hypothesis that the data are not normally distributed is rejected in favor of the alternative. The alternative in this case is that the data are normally distributed.

For example, from Table A4.1, the largest D_i is 0.0681 and the largest D_i' is 0.1557. Thus, the calculated value for D becomes 0.1557. The critical value for D with 35 observations is 0.1480. Since the calculated value for D is larger than the critical value for D, the null hypothesis is rejected. Thus, the data are normally distributed.

A summary of this test, as well as the tests for the general cover types follows. The result of these tests were that the data were normally distributed for the general cover types, both individually and collectively. The null hypothesis (H_o) was that the data were not normally distributed.

ALL GENERAL COVER TYPES COMBINED (FROM TABLE A4.1):

Max D_i = 0.0681 Max D_i' = 0.1557 D = 0.1557

D critical value from statistics table = 0.148

0.1557 > 0.148, therefore, reject H_o. That is, the combined data are normally distributed (α = .05).

FORESTED AREAS (FROM TABLE A4.2):

Max D_i = 0.2382 Max D_i' = 0.4532 D = 0.4532

D critical value from statistics table = 0.350

0.4532 > 0.350, therefore, reject H_o. That is, the data from the forested areas are normally distributed (α = .01).

ROADS/EXPOSED SOIL (FROM TABLE A4.3):

Max D_i = 0.0655 Max D_i' = 0.3243 D = 0.3243

D critical value from statistics table = 0.290

0.3243 > 0.290, therefore, reject H_o. That is, the data from the roads/exposed soil are normally distributed (α = .01).

GRASSLAND AREAS (FROM TABLE A4.4):

Max D_i = 0.1272 Max D_i' = 0.3594 D = 0.3594

D critical value from statistics table = 0.240

0.3594 > 0.240, therefore reject H_o. That is, the data from the grassland areas are normally distributed (α = .01).

Since the data were normally distributed, both individually and collectively, use of the student's t-distribution to test for significant differences in classification accuracy was possible.